# ORIGINAL RESEARCH

Enterohepatic Transcription Factor CREB3L3 Protects Atherosclerosis via SREBP Competitive Inhibition

Yoshimi Nakagawa,[1,2,3,a] Yunong Wang,[1,a] Song-iee Han,[1,2,a] Kanako Okuda,[1] Asayo Oishi,[1] Yuka Yagishita,[1] Kae Kumagai,[1] Hiroshi Ohno,[1] Yoshinori Osaki,[1] Yuhei Mizunoe,[1] Masaya Araki,[1] Yuki Murayama,[1] Hitoshi Iwasaki,[1] Morichika Konishi,[4] Nobuyuki Itoh,[5] Takashi Matsuzaka,[1] Hirohito Sone,[6] Nobuhiro Yamada,[1] and Hitoshi Shimano[1,2,4,7,8]

[1]Department of Internal Medicine (Endocrinology and Metabolism), Faculty of Medicine, University of Tsukuba, Ibaraki; [2]International Institute for Integrative Sleep Medicine (WPI-IIIS), University of Tsukuba, Ibaraki; [3]Division of Complex Bioscience Research, Department of Research and Development, Institute of Natural Medicine, University of Toyama, Toyama; [4]Department of Microbial Chemistry, Kobe Pharmaceutical University, Hyogo; [5]Department of Genetic Biochemistry, Graduate School of Pharmaceutical Science, Kyoto University, Kyoto; [6]Department of Hematology, Endocrinology and Metabolism, Niigata University Faculty of Medicine, Niigata; [7]Life Science Center for Survival Dynamics, Tsukuba Advanced Research Alliance (TARA), University of Tsukuba, Ibaraki; and [8]Japan Agency for Medical Research and Development–Core Research for Evolutional Science and Technology (AMED-CREST), Tokyo, Japan
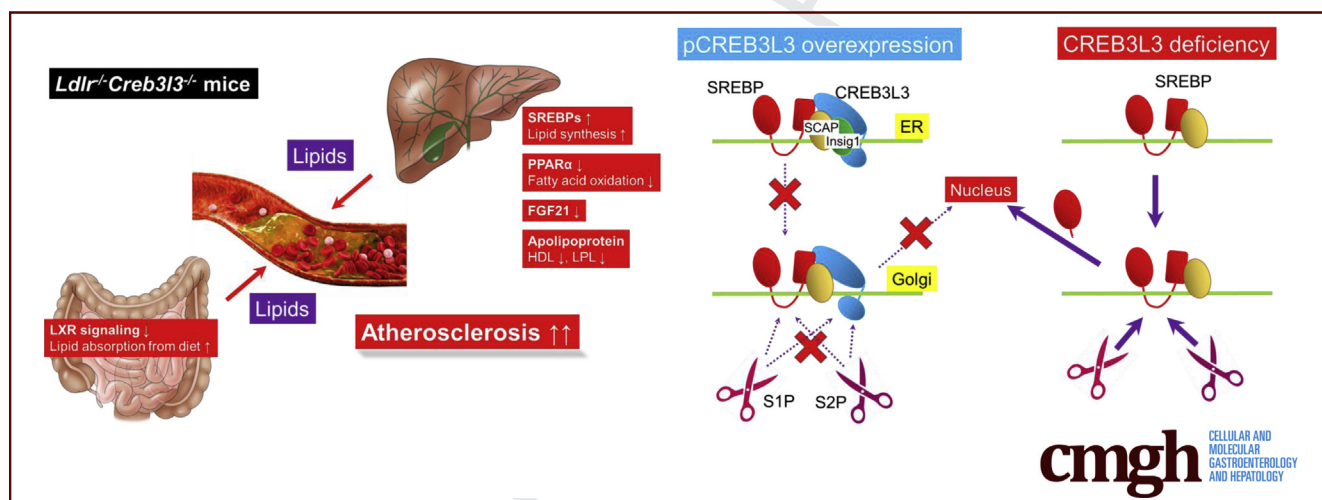
SUMMARY

Deficiency of *CREB3L3* accelerates atherosclerosis, whereas liver CREB3L3 overexpression mice improve atherosclerosis. Hepatic and intestinal CREB3L3 cooperate to regulate whole-body lipid metabolism. Premature CREB3L3 suppresses the intracellular transport from ER to nuclear and the cleavage processes of SREBP.

BACKGROUND & AIMS: cAMP responsive element-binding protein 3 like 3 (CREB3L3) is a membrane-bound transcription factor involved in the maintenance of lipid metabolism in the liver and small intestine. CREB3L3 controls hepatic triglyceride and glucose metabolism by activating plasma fibroblast growth factor 21 (FGF21) and lipoprotein lipase. In this study, we intended to clarify its effect on atherosclerosis.

METHODS: CREB3L3-deficient, liver-specific CREB3L3 knockout, intestine-specific CREB3L3 knockout, both liver- and intestine-specific CREB3L3 knockout, and liver CREB3L3

transgenic mice were crossed with $LDLR^{-/-}$ mice. These mice were fed with a Western diet to develop atherosclerosis.

RESULTS: CREB3L3 ablation in $LDLR^{-/-}$ mice exacerbated hyperlipidemia with accumulation of remnant APOB-containing lipoprotein. This led to the development of enhanced aortic atheroma formation, the extent of which was additive between liver- and intestine-specific deletion. Conversely, hepatic nuclear CREB3L3 overexpression markedly suppressed atherosclerosis with amelioration of hyperlipidemia. CREB3L3 directly upregulates anti-atherogenic FGF21 and APOA4. In contrast, it antagonizes hepatic sterol regulatory element-binding protein (SREBP)–mediated lipogenic and cholesterogenic genes and regulates intestinal liver X receptor–regulated genes involved in the transport of cholesterol. CREB3L3 deficiency results in the accumulation of nuclear SREBP proteins. Because both transcriptional factors share the cleavage system for nuclear transactivation, full-length CREB3L3 and SREBPs in the endoplasmic reticulum (ER) functionally inhibit each other. CREB3L3 promotes the formation of the SREBP-insulin induced gene 1 complex to suppress SREBPs for ER-Golgi transport, resulting in ER retention and inhibition of proteolytic activation at the Golgi and vice versa.

CONCLUSIONS: CREB3L3 has multi-potent protective effects against atherosclerosis owing to new mechanistic interaction between CREB3L3 and SREBPs under atherogenic conditions. *(Cell Mol Gastroenterol Hepatol 2020;■:■–■; https://doi.org/10.1016/j.jcmgh.2020.11.004)*

Keywords: CREB3L3; SREBP; Hyperlipidemia; Enterohepatic Circulation.

C AMP responsive element-binding protein 3 like 3 (*CREB3L3*) is expressed only in the liver and intestinal cells,[1] where the CREB3L3 protein localizes in the endoplasmic reticulum (ER) and is transported to the Golgi apparatus and nucleus.[1–3] Nuclear expression of the active form of CREB3L3 in the nucleus is increased under fasting. This is consistent with the finding that *CREB3L3* mRNA expression is higher during fasting than refeeding.[4] CREB3L3 reduces plasma triglyceride (TG) levels by increasing the hepatic expression of apolipoprotein (Apo)-encoding genes such as apolipoprotein A4 (*Apoa4*), *Apoa5*, and *Apoc2*,[1] which activate blood lipoprotein lipase (LPL) activity. *CREB3L3⁻/⁻* mice exhibit massive hepatic lipid metabolite accumulation and significantly increased plasma TG levels or nonalcoholic steatohepatitis when fed an atherogenic high-fat diet.[5] APOA4 regulates high-density lipoprotein (HDL) metabolism by activating lecithin-cholesterol acyltransferase, a key enzyme involved in cholesterol transfer to newly synthesized HDL particles.[6,7] This leads to stimulation of cholesterol efflux from macrophages[8] and activation of receptor-mediated uptake of HDL by hepatocytes.[9] Overexpression of *APOA4* in mice prevents the development of atherosclerosis.[10–12]

CREB3L3 and peroxisome proliferator-activated receptor alpha (PPARα) synergistically activate hepatic fibroblast growth factor 21 (*Fgf21*) expression.[13,14] Synthesized FGF21 proteins are secreted into the circulation and transported to peripheral tissues. This includes brain and skeletal muscle, as well as white adipose tissue and brown adipose tissue, in which FGF21 activates lipolysis and thermogenesis, respectively.[15] These effects improve diabetes and hyperlipidemia by reducing plasma glucose, insulin, TG, and cholesterol. FGF21 suppresses atherosclerotic development by reducing hypercholesterolemia, oxidative stress, and vascular smooth muscle cell proliferation via adiponectin-dependent and -independent mechanisms.[16,17] FGF21 regulates monocyte and macrophage recruitment, proliferation, and inflammatory functions in bloods and myocardial tissues, preventing macrophage accumulation, inflammation, and fibrosis.[16,18,19]

Recently, it has been shown that CREB3L3 plays a crucial role in lipoprotein metabolism, and *LDLR⁻/⁻CREB3L3⁻/⁻* mice develop significantly more atherosclerotic lesions in the aortas than *LDLR⁻/⁻* mice.[20] However, the contribution of hepatic and intestinal CREB3L3 to atherosclerosis remains unclear. In this study, we revealed that *LDLR⁻/⁻CREB3L3⁻/⁻* mice exhibited severe atherosclerosis by inducing sterol regulatory element-binding protein (SREBP) activation. Liver- and intestine-specific CREB3L3-knockout (KO) in *LDLR⁻/⁻* mice (*LDLR⁻/⁻* LKO and *LDLR⁻/⁻* IKO, respectively) also showed accelerated atherosclerosis formation compared with *LDLR⁻/⁻* mice. Conversely, hepatic CREB3L3 overexpression (TgCREB3L3) in *LDLR⁻/⁻* (*LDLR⁻/⁻*TgCREB3L3) mice suppressed atherosclerosis. Collectively, we propose that CREB3L3 in enterohepatic circulation plays a crucial role in atherosclerosis development, and the mechanism involved in this process warrants further investigation.

Results

CREB3L3 Deletion Promotes Atherosclerosis With Severe Hyperlipidemia at an Early Stage of Western Diet and Irrespective of Sex

To evaluate the early stage of atherosclerosis in *LDLR⁻/⁻CREB3L3⁻/⁻* mice, female and male *LDLR⁻/⁻CREB3L3⁻/⁻* mice were fed a Western diet (WD) for 5 weeks. The *LDLR⁻/⁻CREB3L3⁻/⁻* mice showed a significant increase in atherosclerotic lesion formation in both the entire aorta and aortic root compared with control *LDLR⁻/⁻* mice, which showed barely detectable lesions at this stage (Figures 1*A* and *B*, 2*A* and *B*). Plasma TG, total cholesterol (TC), total bile acid (TBA), and free fatty acid (FFA) levels were markedly higher in female and male *LDLR⁻/⁻CREB3L3⁻/⁻* mice than in *LDLR⁻/⁻* mice (Figures 1*C* and *D*, 2*C* and *D*). High-performance liquid chromatography (HPLC) analysis revealed marked accumulation of TG and cholesterol and significant enrichment of APOB-containing lipoprotein fractions in female and male *LDLR⁻/⁻CREB3L3⁻/⁻* mice (Figures 1*C* and 2*C*). Significant increases in very-low-density lipoprotein (VLDL)-APOB proteins (APOB100 and APOB40) were observed in female and male *LDLR⁻/⁻CREB3L3⁻/⁻* mice relative to *LDLR⁻/⁻* mice (Figures 1*C* and 2*C*). Overexpression of APOA4, a target of CREB3L3,[21] has been reported to possess anti-atherogenic properties.[10–12] Plasma APOA4 levels in *LDLR⁻/⁻CREB3L3⁻/⁻* mice were significantly lower than those measured in *LDLR⁻/⁻* mice (Figures 1*C* and 2*C*). Plasma levels of FGF21, an anti-atherogenic hormone, were significantly reduced in female and male *LDLR⁻/⁻CREB3L3⁻/⁻* mice (Figures 1*D* and 2*D*). Collectively, we hypothesized that the absence of CREB3L3 induced severe combined hyperlipidemia with

pro-atherogenic plasma lipoprotein and hormonal profiles. Of note, the atherosclerosis lesions were fewer but clearly visible in both female and male $LDLR^{-/-}CREB3L3^{-/-}$ mice even when they consumed a normal diet, which gave rise to almost negligible atheroma in $LDLR^{-/-}$ mice (Figure 3A, B, D, and E). Plasma TG, TC, and FFA levels were markedly higher in female and male $LDLR^{-/-}CREB3L3^{-/-}$ mice than in $LDLR^{-/-}$ mice (Figure 3C and D). Plasma TBA

5 weeks Female
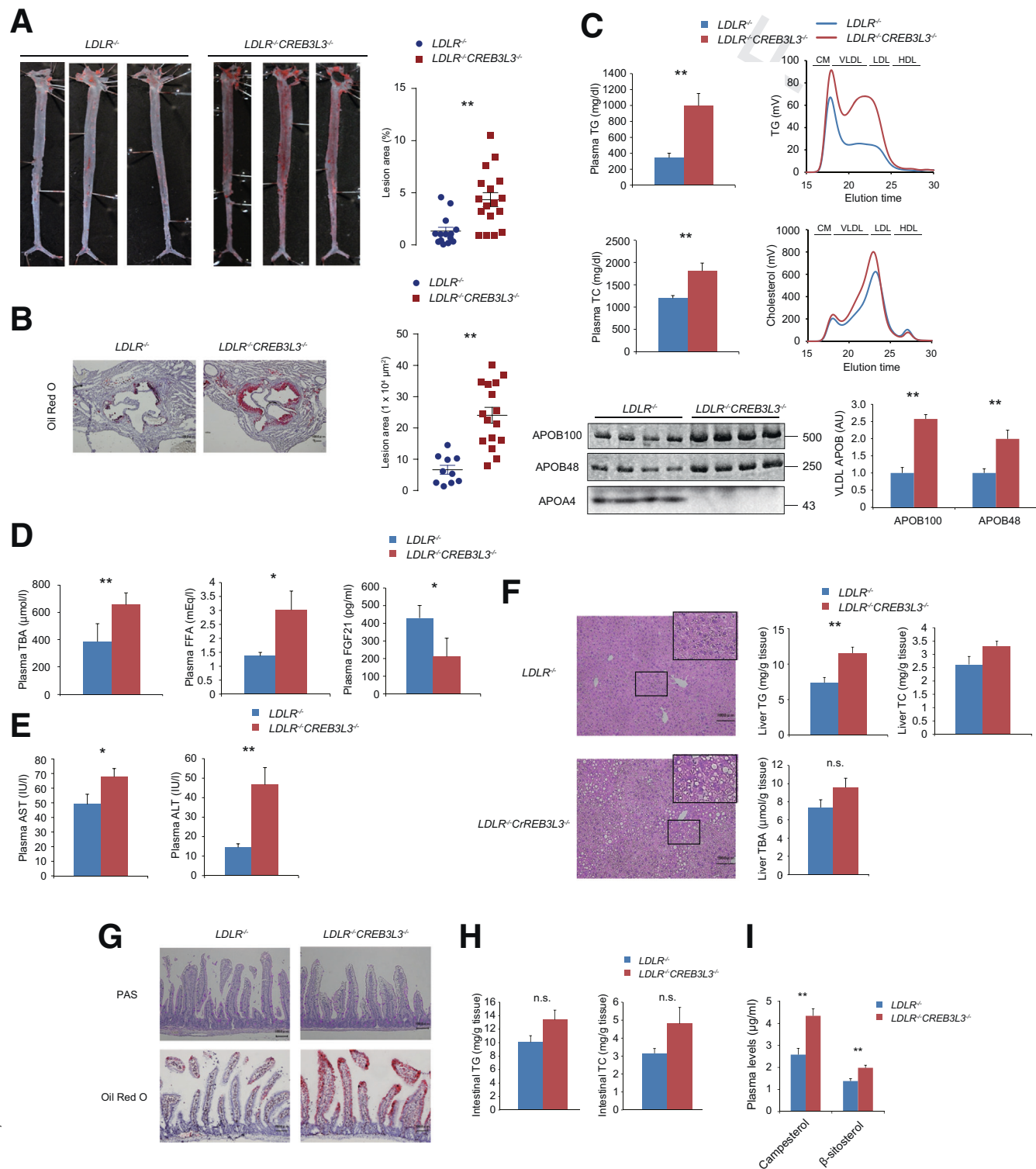
levels were higher in female $LDLR^{-/-}CREB3L3^{-/-}$ mice than in $LDLR^{-/-}$ mice but reversed in male $LDLR^{-/-}CREB3L3^{-/-}$ mice (Figure 3C and D).

Deficiency of CREB3L3 Dysregulates Hepatic Lipid Metabolism and Subsequently Exacerbates Steatohepatitis

Plasma aspartate aminotransferase and alanine aminotransferase levels were also increased (Figure 1E), suggesting more severe liver injury in $LDLR^{-/-}CREB3L3^{-/-}$ mice versus $LDLR^{-/-}$ mice. Histologic liver sections from female and male $LDLR^{-/-}CREB3L3^{-/-}$ mice exhibited severe lipid accumulation (Figures 1F and 2E). Liver TG and TC levels in female and male $LDLR^{-/-}CREB3L3^{-/-}$ mice were higher than those of $LDLR^{-/-}$ mice (Figures 1F and 2E). Liver TBA levels in female $LDLR^{-/-}CREB3L3^{-/-}$ mice tended to decrease but not significantly, and there was no change between male genotypes (Figures 1F and 2E). These findings support that $LDLR^{-/-}CREB3L3^{-/-}$ mice increase de novo lipogenesis and hepatosteatosis. Taken together, we found that $LDLR^{-/-}CREB3L3^{-/-}$ mice develop both atherosclerosis and hepatosteatosis, regardless of sex differences. Therefore, the disruption of CREB3L3 is a very strong risk factor for the onset and progression of arteriosclerosis. Subsequently, we mainly used female mice for the study of KO mice.

Deletion of CREB3L3 in the Small Intestine Promotes Lipid Absorption From Diet, Contributing to Hyperlipidemia

CREB3L3 is also expressed in the intestines. Histologic analysis with periodic acid–Schiff staining did not reveal differences in small intestinal mucin-producing goblet cells (Figure 1G). However, enhanced lipid accumulation in the villi of female $LDLR^{-/-}CREB3L3^{-/-}$ mice fed a WD for 5 weeks were detected and quantitatively confirmed (Figure 1G and H). This evidence suggested that there is a dysregulation of lipid metabolism in the small intestines of $LDLR^{-/-}CREB3L3^{-/-}$ mice. The levels of cholesterol absorption markers, such as campesterol and β-sitosterol,[22] in the plasma of $LDLR^{-/-}CREB3L3^{-/-}$ mice were significantly higher than those observed in $LDLR^{-/-}$ mice (Figure 1I).

Hence, *CREB3L3* deletion in the small intestine may cause an increase in intestinal cholesterol absorption, thus exacerbating hyperlipidemia. $LDLR^{-/-}CREB3L3^{-/-}$ mice showed an apparent increase in chylomicron production (Figure 4), supporting the notion that deficiency of CREB3L3 increases the activity of TG absorption in the intestine and subsequent chylomicron-TG production. Taken together, CREB3L3 deletion in the small intestine contributes to hyperlipidemia. Conversely, as we previously reported, intestinal CREB3L3-overexpressing mice exhibited suppression of plasma TC levels when fed the same diet via the suppression of cholesterol absorption in the intestine.[23] These findings indicate that hepatic CREB3L3 regulates TG metabolism, and that intestinal CREB3L3 regulates cholesterol and TG absorption in the small intestine, further suggesting that CREB3L3 regulates systemic lipid metabolism in enterohepatic circulation.

Arteriosclerosis Is Exacerbated in $LDLR^{-/-}$ $CREB3L3^{-/-}$ Mice After WD Feeding for 3 Months, a Standard Condition of the Evaluation

$LDLR^{-/-}CREB3L3^{-/-}$ mice exhibited early severe atherosclerosis and remained in these phenotypes even after a WD feeding for 3 months. Similar to the observation after the 5-week diet, female $LDLR^{-/-}CREB3L3^{-/-}$ mice revealed a significant increase in atherosclerotic lesion formation (Figure 5A and B). Plasma lipid levels were markedly higher in $LDLR^{-/-}CREB3L3^{-/-}$ mice than in $LDLR^{-/-}$ mice (Figure 5C and D), accompanied by a marked accumulation of both TG in the chylomicron, VLDL, intermediate density lipoprotein, and low-density lipoprotein fractions, and the entire APOB-containing lipoproteins of $LDLR^{-/-}CREB3L3^{-/-}$ mice (Figure 5C). Plasma FGF21 levels of $LDLR^{-/-}CREB3L3^{-/-}$ mice were significantly lower than those of $LDLR^{-/-}$ mice (Figure 5D). These findings indicate that even after feeding with a WD for 3 months, deficiency of *CREB3L3* leads to the development of severe atherosclerosis with severe combined hyperlipidemia.

Liver and Intestine CREB3L3 Deficiencies Additively Develop Atherosclerosis

To define the tissue-specific contribution of CREB3L3 in the suppression of atherosclerosis, CREB3L3 LKO and IKO mice[24] were crossed with $LDLR^{-/-}$ mice, generating $LDLR^{-/-}$

Figure 1. (*See previous page*). **A WD for 5 weeks promotes atherosclerosis in $LDLR^{-/-}$ $CREB3L3^{-/-}$ mice.** Ten- to 11-week-old female $LDLR^{-/-}$ and $LDLR^{-/-}CREB3L3^{-/-}$ mice were fed a WD for 5 weeks. Samples were collected in a fed state. (A) Representative images of entire Sudan IV-stained aortas from $LDLR^{-/-}$ (n = 14) and $LDLR^{-/-}CREB3L3^{-/-}$ (n = 17) mice. Surface area occupied by lesions was quantified. **P < .01 vs $LDLR^{-/-}$ mice. (B) Representative aortic root sections from $LDLR^{-/-}$ (n = 10) and $LDLR^{-/-}CREB3L3^{-/-}$ (n = 16) mice. Cross sections were stained with Oil Red O and hematoxylin. Aortic root lesion areas were quantified. **P < .01 vs $LDLR^{-/-}$ mice. (C) Plasma TG and TC levels (n = 7, respectively). HPLC analysis of plasma lipoprotein profiles specific for plasma TG and cholesterol. APOB100 and APOB48 in VLDL fractions and its quantification (n = 7, respectively). **P < .01 vs $LDLR^{-/-}$ mice. Plasma APOA4 levels. (D) Plasma levels of TBA (n = 7 each), FFA (n = 7 each), and FGF21 (n = 5–6 per group). *P < .05 vs $LDLR^{-/-}$ mice. (E) Plasma aspartate and alanine aminotransferase (AST and ALT) levels. n = 9–10 per group. *P < .05 and **P < .01 vs $LDLR^{-/-}$ mice. (F) Histology of liver sections and liver TG, TC, and TBA levels (n = 5–8 per group). *P < .05 and **P < .01 vs $LDLR^{-/-}$ mice. (G) Hematoxylin-eosin staining, Oil Red O staining, and periodic acid–Schiff (PAS) staining of small intestines from these mice. (H) Intestinal TG and TC levels of these mice (n = 6–8 per group). (I) Quantification of campesterol and β-sitosterol levels of female mice (n = 7–8 per group). **P < .01 vs $LDLR^{-/-}$ mice. CM, control mice.
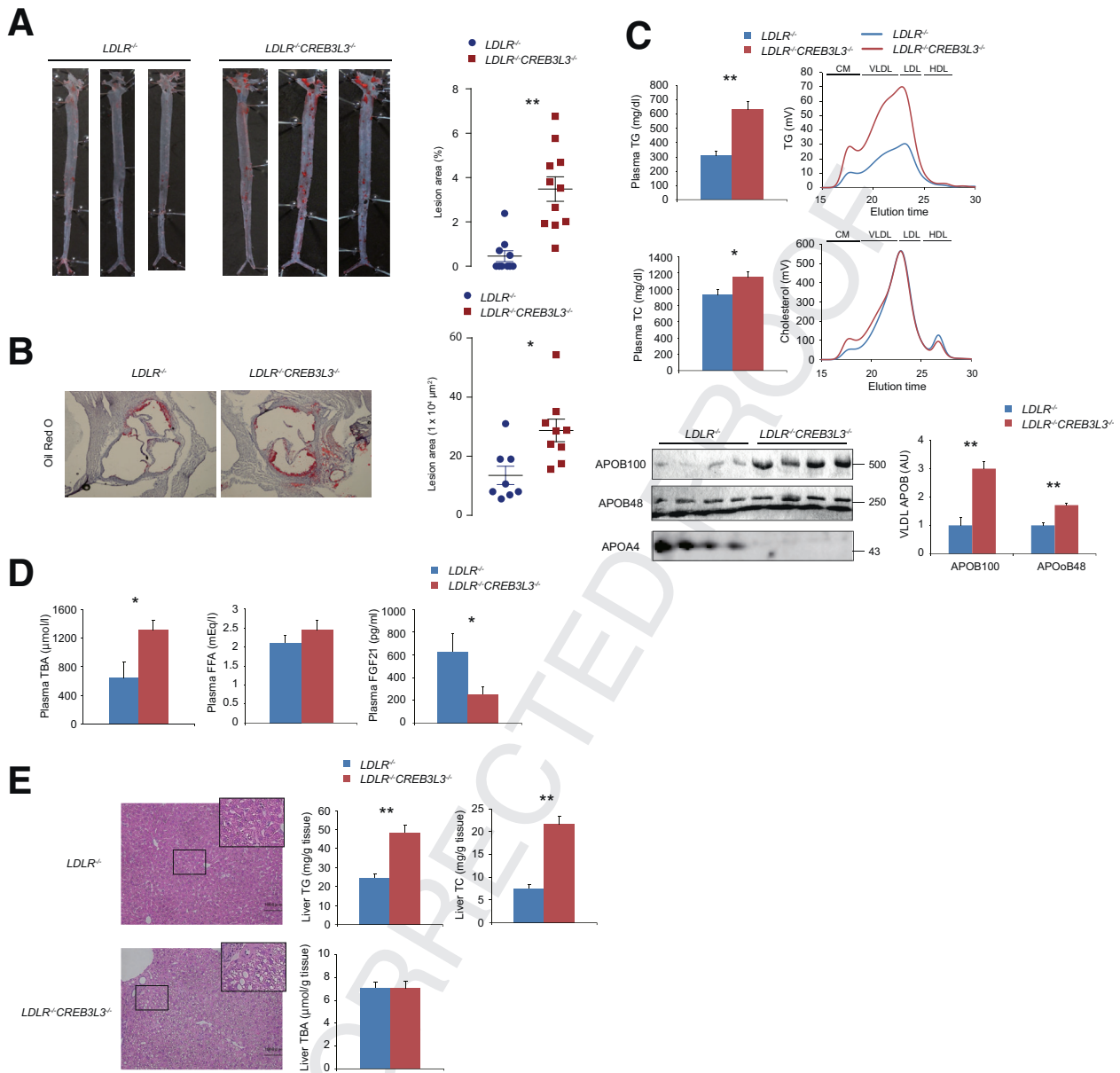
5 weeks male

Figure 2. A WD for 5 weeks promotes atherosclerosis in male $LDLR^{-/-}$ $CREB3L3^{-/-}$ mice. Ten- to 11-week-old male $LDLR^{-/-}$ and $LDLR^{-/-}CREB3L3^{-/-}$ mice were fed a WD for 5 weeks. Samples were collected in a fed state. (*A*) Representative images of entire Sudan IV-stained aortas from $LDLR^{-/-}$ (n = 11) and $LDLR^{-/-}CREB3L3^{-/-}$ (n = 11) mice. Surface area occupied by lesions was quantified. **$P <$ .01 vs $LDLR^{-/-}$ mice. (*B*) Representative aortic root sections from $LDLR^{-/-}$ (n = 11) and $LDLR^{-/-}CREB3L3^{-/-}$ (n = 11) mice. Cross sections were stained with Oil Red O and hematoxylin. Aortic root lesion areas were quantified. *$P <$ .05 vs $LDLR^{-/-}$ mice. (*C*) Plasma TG and TC levels (n = 11 each). HPLC analysis of plasma lipoprotein profiles specific for plasma TG and cholesterol. APOB100 and APOB48 were isolated from VLDL fractions via ultracentrifugation, subjected to sodium dodecyl sulfate–polyacrylamide gel electrophoresis, stained with Coomassie Brilliant Blue, and quantified. n = 6–7 per group. *$P <$ .05 and **$P <$ .01 vs $LDLR^{-/-}$ mice. Plasma APOA4 levels were determined by Western blotting. (*D*) Plasma TBA, FFA, and FGF21 levels. n = 5–11 per group. *$P <$ .05 vs $LDLR^{-/-}$ mice. (*E*) Histology of liver sections, and liver TG, TC, and TBA levels. n = 9–15 per group. *$P <$ .05 vs $LDLR^{-/-}$ mice. CM, control mice.

CREB3L3 LKO and $LDLR^{-/-}$CREB3L3 IKO mice, respectively. By further crossing of these mice, $LDLR^{-/-}$ mice specifically deficient in both liver and intestine CREB3L3 ($LDLR^{-/-}$CREB3L3 DKO) were generated. The general plasma biochemical phenotypes of these mice on a normal diet were

evaluated at 8 weeks; both $LDLR^{-/-}$CREB3L3 LKO and $LDLR^{-/-}$CREB3L3 IKO mice showed higher plasma TG levels than $LDLR^{-/-}$flox mice (Figure 6A). Plasma TC levels of $LDLR^{-/-}$CREB3L3 LKO were significantly higher; however, the levels of $LDLR^{-/-}$CREB3L3 IKO mice were not changed
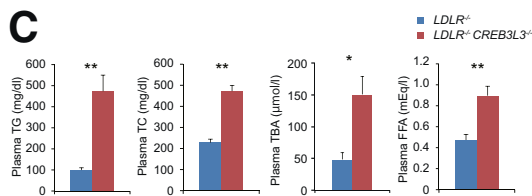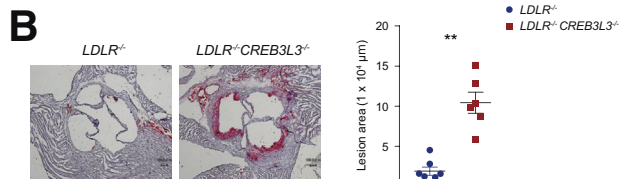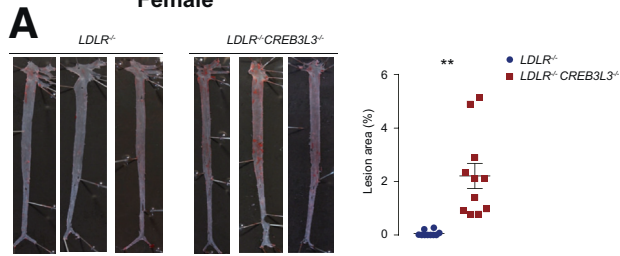
Figure 3. Even feeding with normal diet promotes atherosclerosis in $LDLR^{-/-}CREB3L3^{-/-}$ mice. Sixteen-week-old female (*A–C*) and male (*D–F*) $LDLR^{-/-}$ and $LDLR^{-/-}CREB3L3^{-/-}$ mice were fed a normal diet. Samples were collected in a fed state. (*A*) Representative aortic root sections from female $LDLR^{-/-}$ (n = 10) and $LDLR^{-/-}CREB3L3^{-/-}$ (n = 11) mice. Cross sections were stained with Oil Red O and hematoxylin. Aortic lesion areas were quantified. **$P < .01$ vs $LDLR^{-/-}$ mice. (*B*) Representative images of entire Sudan IV-stained aortas from $LDLR^{-/-}$ (n = 7) and $LDLR^{-/-}CREB3L3^{-/-}$ (n = 6) mice. Surface area occupied by lesions was quantified. **$P < .01$ vs $LDLR^{-/-}$ mice. (*C*) Plasma TG, TC, TBA, and FFA levels of female $LDLR^{-/-}$ and $LDLR^{-/-}CREB3L3^{-/-}$ mice (n = 5–8 per group). **$P < .01$ vs $LDLR^{-/-}$ mice. (*D*) Representative aortic root sections from male $LDLR^{-/-}$ (n = 15) and $LDLR^{-/-}CREB3L3^{-/-}$ (n = 17) mice. Cross sections were stained with Oil Red O and hematoxylin. Aortic lesion areas were quantified. **$P < .01$ vs $LDLR^{-/-}$ mice. (*E*) Representative images of entire Sudan IV-stained aortas from male $LDLR^{-/-}$ (n = 7) and $LDLR^{-/-}CREB3L3^{-/-}$ (n = 10) mice. Surface area occupied by lesions was quantified. *$P < .05$ vs $LDLR^{-/-}$ mice. (*F*) Plasma TG, TC, TBA, and FFA levels of male $LDLR^{-/-}$ and $LDLR^{-/-}CREB3L3^{-/-}$ mice (n = 11–16 per group). *$P < .05$ and **$P < .01$ vs $LDLR^{-/-}$ mice.

compared with those of $LDLR^{-/-}$ flox mice. $LDLR^{-/-}CREB3L3$ DKO mice showed increases in both plasma TG and TC levels additively with liver and small intestine defects (Figure 6*B*). HPLC analysis exhibited higher plasma TG and cholesterol levels, which were distributed over APOB-containing lipoproteins in the following order: DKO, LKO, IKO, and flox mice (Figure 6*A* and *B*). $LDLR^{-/-}CREB3L3$ DKO particularly showed a peak in the chylomicron fraction and a decrease in HDL cholesterol. The pattern of plasma FFA levels was similar to that of plasma TG levels (Figure 6*C*). The pattern of plasma TBA levels was similar to that of plasma TC levels (Figure 6*C*), suggesting that liver CREB3L3 deletion leads to bile acid metabolism disorders. Plasma FGF21 levels of $LDLR^{-/-}CREB3L3$ LKO and $LDLR^{-/-}CREB3L3$ DKO mice were significantly lower than those of $LDLR^{-/-}$ flox mice (Figure 6*C*), indicating that these levels were dependent on hepatic CREB3L3 in contrast to the contribution of CREB3L3 of both organs to plasma lipids. Collectively, the data indicate that both liver and intestine CREB3L3 additively contribute to lipid metabolism.

After feeding the mice with a WD for 3 months, atherosclerotic lesion areas in all groups of KO mice were greater than those recorded in control flox mice. Increases in the estimations by both the entire area and cross section at the sinus were as follows (ascending order): IKO, LKO, and DKO mice (Figure 7*A* and *B*). Because of the absence of both liver and intestine CREB3L3, the development of atherosclerosis was further exacerbated in $LDLR^{-/-}CREB3L3$ DKO mice. This effect was presumably induced by the absence of both collaboratively disturbing lipid metabolism and atherogenic risks (Figure 7*A* and *B*).

Hepatic CREB3L3 Activation Suppresses the Formation of Atherosclerotic Lesions in $LDLR^{-/-}$ Mice That Were Fed a WD

Mice with hepatic overexpression of active CREB3L3 (TgCREB3L3) (Figure 8)[14] were crossed with $LDLR^{-/-}$ mice. $LDLR^{-/-}$ and $LDLR^{-/-}$TgCREB3L3 mice were fed a WD for 3 months and subsequently subjected to an atherosclerosis analysis. Lesions were markedly suppressed in both the
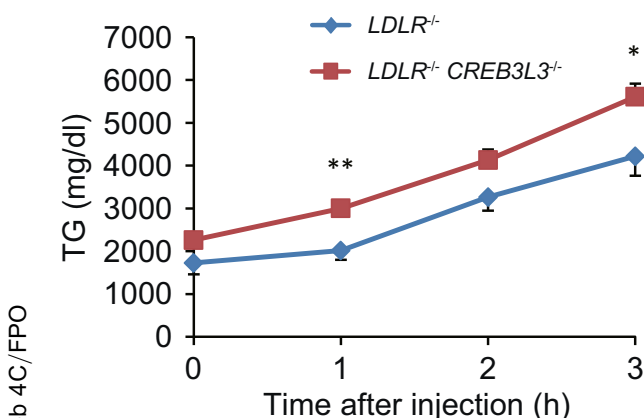
web 4C/FPO

Figure 4. $LDLR^{-/-}CREB3L3^{-/-}$ **mice show increased intestinal TG absorption.** Eight-week-old female LDLR−/− and LDLR−/−CREB3L3−/− mice were fasted for 3 hours and intravenously injected with Triton WR-1339. After injection (2 hours), mice received 100 μL olive oil orally. Plasma was collected at 0, 1, 2, and 3 hours after administration. n = 7 each. *$P < .05$ and **$P < .01$ vs $LDLR^{-/-}$ mice.

entire aorta and aortic root of $LDLR^{-/-}$TgCREB3L3 mice (Figure 9A and B), indicating that hepatic CREB3L3 over-expression attenuates the WD-induced development of atherosclerosis. In addition, because FGF21 (a main CREB3L3 target) exerts a protective effect against athero-sclerosis, the contribution of FGF21 in these phenotypes was estimated by crossing $LDLR^{-/-}$TgCREB3L3 mice with $FGF21^{-/-}$ mice to generate $LDLR^{-/-}$TgCREB3L3$FGF21^{-/-}$ mice, followed by being fed on a WD diet for 3 months. Deletion of FGF21 was confirmed by showing that plasma FGF21 levels were significantly increased in $LDLR^{-/-}$TgCREB3L3 mice and not detected in $FGF21^{-/-}$ back-ground mice (Figure 9C). Consistent with a previous report,[16] $LDLR^{-/-}FGF21^{-/-}$ mice showed a trend of more severe development of atherosclerosis. However, $LDLR^{-/-}FGF21^{-/-}$ TgCREB3L3 mice maintained a significant sup-pression of atherosclerosis to a similar extent in the pres-ence of FGF21. Notably, the inhibition rate by CREB3L3 overexpression was estimated to be approximately 50% and 40% in $LDLR^{-/-}$ and $LDLR^{-/-}FGF21^{-/-}$ mice, respectively (Figure 9A and B). These data suggested that the anti-atherogenic effect of CREB3L3 is not mediated primarily through FGF21. CREB3L3 overexpression significantly reduced the plasma TG, TBA, and FFA levels of $LDLR^{-/-}$ mice and $LDLR^{-/-}FGF21^{-/-}$ mice. There were no differ-ences in plasma TC levels among all genotypes (Figure 9C). As a causative factor for hyperlipidemia and atherosclerosis in a previous report,[1] plasma levels of APOA4, an LPL modulator, and a CREB3L3 target gene,[1] were similarly increased in mice overexpressing CREB3L3 among both $LDLR^{-/-}$TgCREB3L3 and $LDLR^{-/-}FGF21^{-/-}$TgCREB3L3 mice (Figure 9D). In gain of function, CREB3L3 target APOA4, but not FGF21, contributed to the suppressive ef-fects of hepatic CREB3L3 on the development of athero-sclerosis. Taken together with the observations in KO mice, it can be concluded that CREB3L3 prevents atherosclerosis.

CREB3L3 Regulates TG Metabolism by Controlling Apolipoproteins in the Liver of $LDLR^{-/-}$ Mice

We next investigated the potential risk factors linked to atherosclerosis-prone CREB3L3 deficiency, starting with TG metabolism. VLDL secretions from the liver were signifi-cantly increased in $LDLR^{-/-}CREB3L3^{-/-}$ mice (Figure 10A). Consistent with a previous study,[1] the expression of LPL activators (eg, Apoc2 and Apoa5) was significantly reduced in $LDLR^{-/-}CREB3L3^{-/-}$ mice, whereas the expression of the LPL inhibitor Apoc3 was increased (Figure 11A). One of the LPL activators, Apoa4, tended to decrease but not signifi-cantly (Figure 11A). These changes contribute to hyper-triglyceridemia by inhibiting LPL activity and impairing TG clearance. In accordance with the decreased plasma LPL activity, TG clearance was remarkably decreased in $LDLR^{-/-}CREB3L3^{-/-}$ mice (Figure 10B and C).

In contrast to $LDLR^{-/-}CREB3L3^{-/-}$ mice, hepatic CREB3L3 overexpression significantly increased hepatic Apoa4 and Apoc2 expression (Figure 11B). Consistent with a previous report,[25] CREB3L3 overexpression increased bile acid synthesis-related gene expression, including that of cytochrome P450 family 7 subfamily A member 1 (Cyp7a1) and Cyp8b1 (Figure 11B). Cyp7a1 and Cyp8b1 were regu-lated by FXR/SHP signaling,[26] but Fxr and Shp were not changed in both $LDLR^{-/-}CREB3L3^{-/-}$ and $LDLR^{-/-}$ TgCREB3L3 mice compared with $LDLR^{-/-}$ mice (Figure 11A and B). $LDLR^{-/-}$TgCREB3L3 mice exhibited an apparent increase in TG clearance (Figure 10E) but no difference in VLDL secretions compared with $LDLR^{-/-}$ mice (Figure 10D). There was no difference in plasma LPL ac-tivity between $LDLR^{-/-}$ and $LDLR^{-/-}$TgCREB3L3 mice (Figure 10F). However, changes in apolipoproteins could partially modulate plasma LPL activity and lead to a consequent decrease in plasma TG-rich lipoprotein levels. FGF21 also has the ability to reduce plasma TG levels.[27] Our findings suggest that CREB3L3 activates FGF21 and LPL regulatory genes, resulting in a reduction in plasma TG levels.

Deficiency of CREB3L3 in the Small Intestine of $LDLR^{-/-}$ Mice Dysregulates Liver X Receptor Signaling

Next we focused on intestinal lipid metabolism. The expression of $LXR\alpha/\beta$ and liver X receptor (LXR) signaling molecules, adenosine triphosphate binding cassette subfamily A member 1 (Abca1), Abcg5, and Abcg8, was significantly down-regulated in the intestines of $LDLR^{-/-}CREB3L3^{-/-}$ mice. In contrast, the expression of Abcg1 tended to decrease, but not significantly (Figure 11C). Fxr and Shp were not changed (Figure 11C). On the basis of a previous report demonstrating that intestinal overexpression of active LXRα in $LDLR^{-/-}$ ($LDLR^{-/-}$TgLXRα) mice improves atherosclerosis,[28] we also speculated that the suppression of LXR signaling in intestines of $LDLR^{-/-}CREB3L3^{-/-}$ mice contributes to the acceleration of atherosclerosis. $LDLR^{-/-}$TgLXRα mice consis-tently exhibited significantly reduced intestinal cholesterol absorption.[28] Therefore, the increase in intestinal cholesterol

web 4C/FPO

3 months Female

A

B

C

D

web 4C/FPO
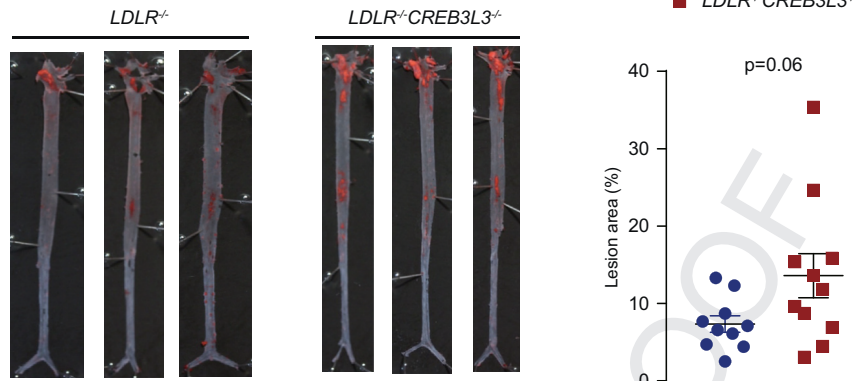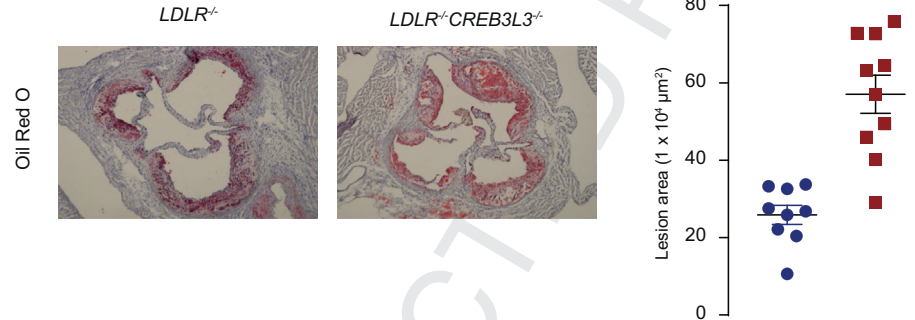
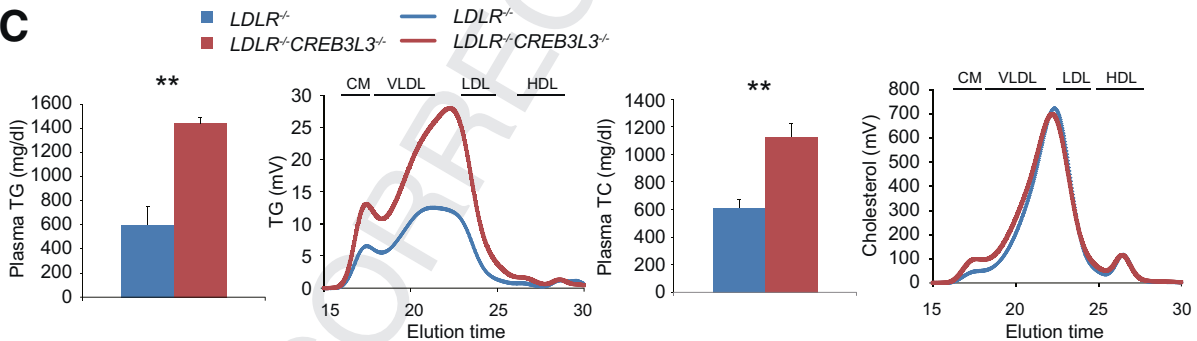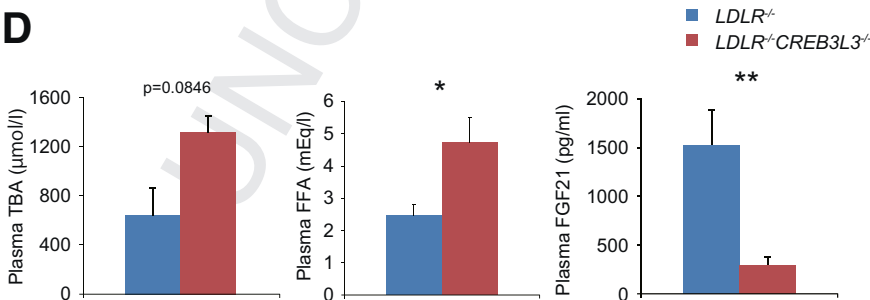**Figure 5. A WD for 3 months promotes atherosclerosis in $LDLR^{-/-}$ $CREB3L3^{-/-}$ mice.** Ten- to 11-week-old female $LDLR^{-/-}$ and $LDLR^{-/-}CREB3L3^{-/-}$ mice were fed a WD for 3 months. Samples were collected in a fed state. (*A*) Representative images of entire Sudan IV-stained aortas from $LDLR^{-/-}$ (n = 10) and $LDLR^{-/-}CREB3L3^{-/-}$ (n = 11) mice. Surface area occupied by lesions was quantified. (*B*) Representative aortic root sections from $LDLR^{-/-}$ (n = 9) and $LDLR^{-/-}CREB3L3^{-/-}$ (n = 10) mice. Cross sections were stained with Oil Red O and hematoxylin. Aortic root lesion areas were quantified. **$P < .01$ vs $LDLR^{-/-}$ mice. (*C*) Plasma TG (n = 6–7) and TC (n = 11 each) levels. HPLC analysis of plasma lipoprotein profiles specific for plasma TG and cholesterol. **$P < .01$ vs $LDLR^{-/-}$ mice. (*D*) Plasma TBA, FFA, and FGF21 levels (n = 10–11 per group). *$P < .05$ and **$P < .01$ vs $LDLR^{-/-}$ mice. CM, control mice.
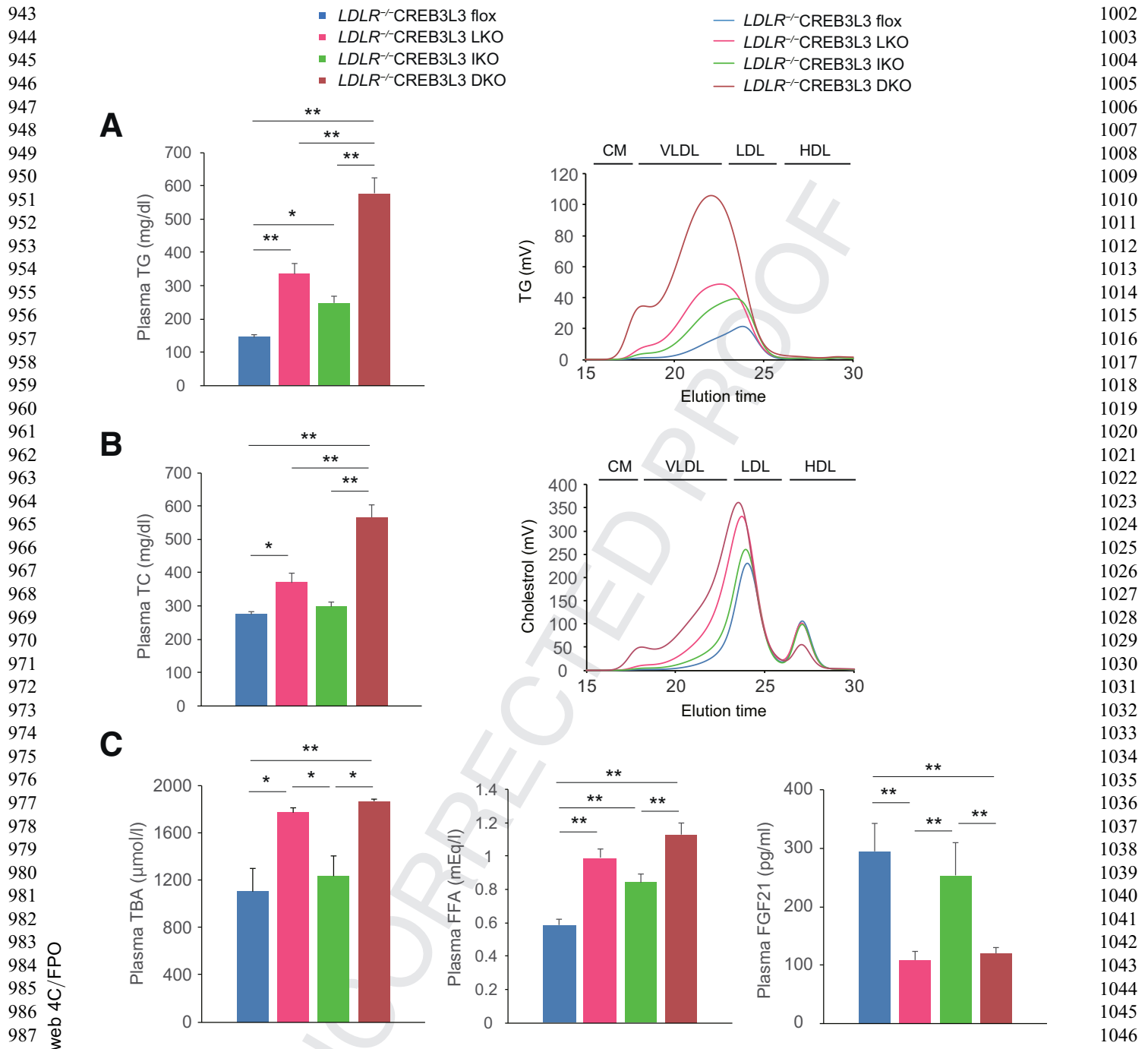
Figure 6. Plasma lipoprotein profiles in female *LDLR*⁻/⁻ mice after deletion of tissue-specific *CREB3L3.* Samples were collected from 8-week-old female *LDLR*⁻/⁻ CREB3L3 flox, *LDLR*⁻/⁻ CREB3L3 LKO, *LDLR*⁻/⁻ CREB3L3 IKO, and *LDLR*⁻/⁻ CREB3L3 DKO mice in a fed state. (*A* and *B*) Plasma TG (*A*) and TC (*B*) levels (n = 17–29 per group). *$P < .05$ and **$P < .01$ among genotypes. HPLC analysis of plasma lipoprotein profiles of TG and cholesterol. (*C*) Plasma levels of TBA (n = 6–7 each), FFA (n = 18–25 per group), and FGF21 (n = 16–17 per group). **$P < .01$ among genotypes.

absorption in *LDLR*⁻/⁻ *CREB3L3*⁻/⁻ mice may depend on the down-regulation of LXR signaling in the small intestine. Reductions in *Abcg5/8*, which increased cholesterol excretion into the intestinal lumen, also led to accumulation of cholesterol in the intestines of *LDLR*⁻/⁻ *CREB3L3*⁻/⁻ mice. Similar to the liver, *Apoa4* and *Apoc2* expression was decreased in the small intestines of *LDLR*⁻/⁻ *CREB3L3*⁻/⁻ mice (Figure 11*C*).

Deficiency of CREB3L3 Activates the Hepatic Expression of SREBP-1 and -2 Target Genes in the Liver of LDLR⁻/⁻ Mice

To further investigate the integral mechanism, we determined the hepatic gene expression profiles of *CREB3L3*⁻/⁻ and hepatic transgenic (Tg) mice. Consistent with the previously described profiles of *CREB3L3*⁻/⁻
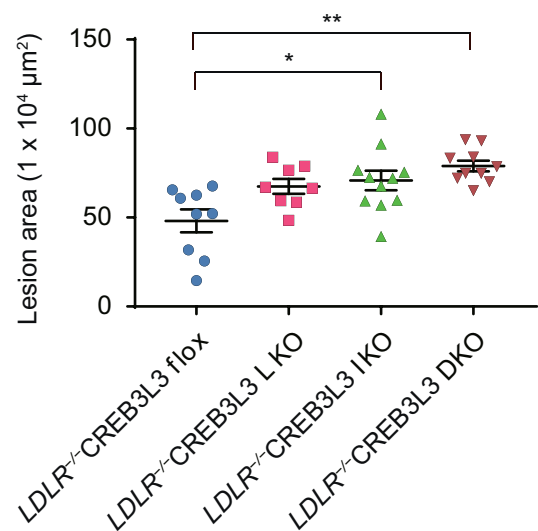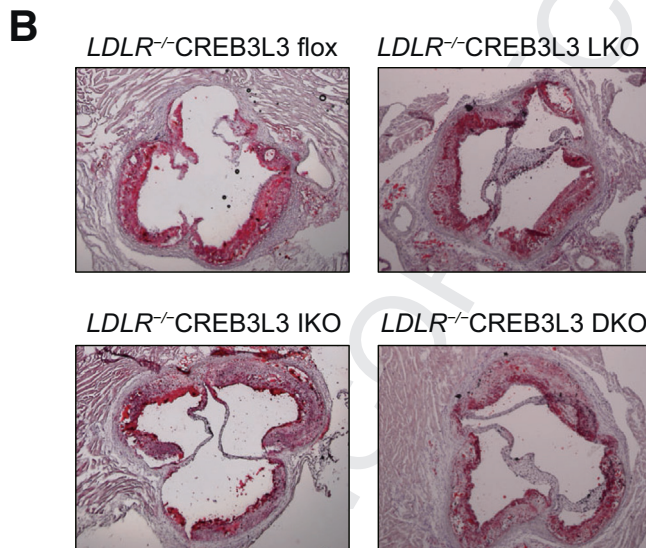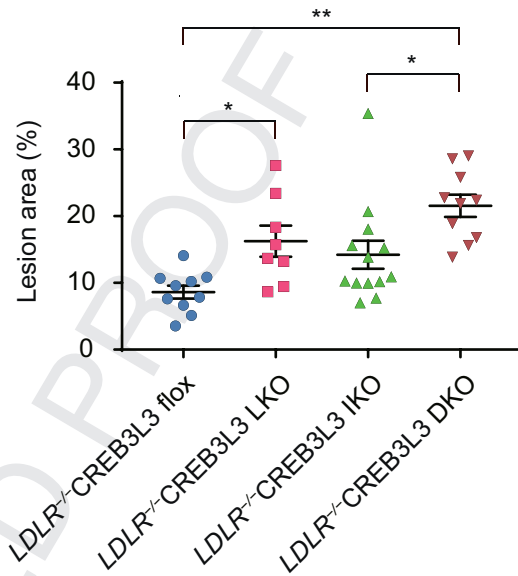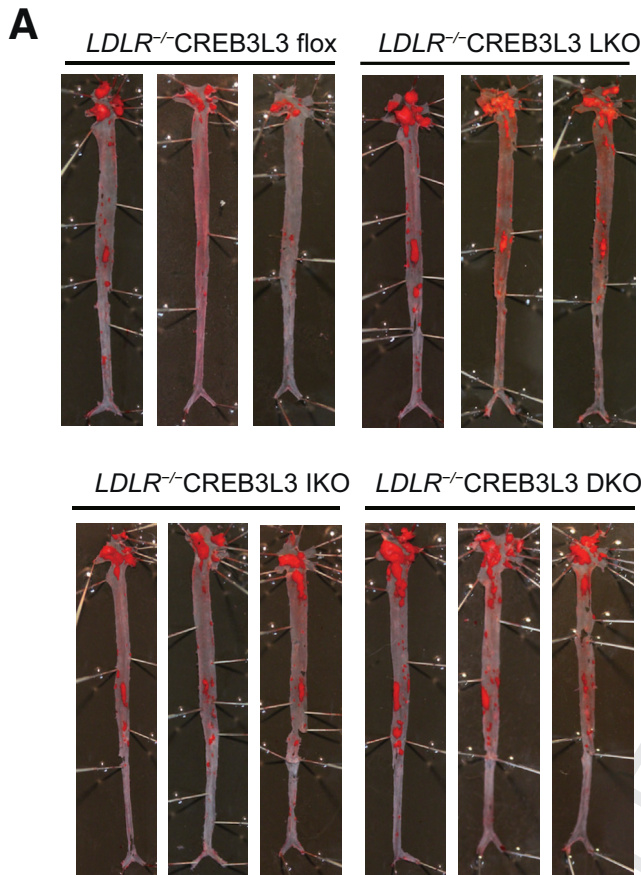
A

B

Figure 7. A WD for 3 months exacerbates development of atherosclerosis after deletion of tissue-specific *CREB3L3* in *LDLR*^−/− mice fed. Ten- to 11-week-old female *LDLR*^−/−flox (flox), *LDLR*^−/−liver-specific *CREB3L3* knockout (LKO), *LDLR*^−/−intestine-specific *CREB3L3* knockout (IKO), and *LDLR*^−/−liver- and intestine-specific *CREB3L3* knockout (DKO) mice were fed a WD for 3 months; samples were collected in a fed state. (*A*) Representative images of entire Sudan IV-stained aortas from flox (n = 10), LKO (n = 8), IKO (n = 13), and DKO (n = 10) mice. Surface area occupied by the lesions was quantified. *$P <$ .05 and **$P <$ .01 among genotypes. (*B*) Representative aortic root sections from flox (n = 9), LKO (n = 8), IKO (n = 11), and DKO (n = 10) mice. Cross sections were stained with Oil Red O and hematoxylin. Aortic root lesion areas were quantified. *$P <$ .05 and **$P <$ .01 among genotypes.
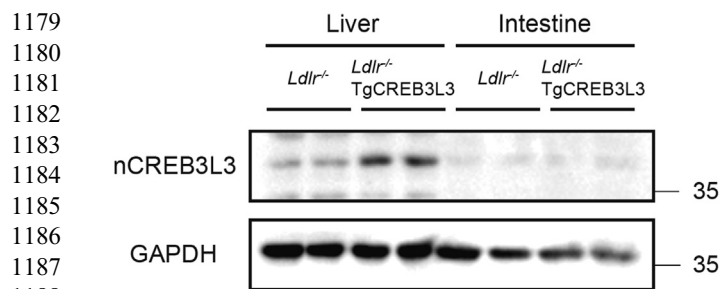
web 4C/FPO

Figure 8. Ectopic active form of CREB3L3 protein in the liver and intestine of $LDLR^{-/-}$TgCREB3L3 mice. Levels of the ectopic active form of CREB3L3 protein in the liver and small intestine of 8-week-old male $LDLR^{-/-}$ and $LDLR^{-/-}$TgCREB3L3 mice were determined by Western blotting.

mice,[14] genes downstream of CREB3L3, including fatty acid oxidation-related genes (eg, *Ppara*), carnitine palmitoyltransferase 1a, liver (*Cpt1a*), and *Fgf21*, were decreased in $LDLR^{-/-}CREB3L3^{-/-}$ mice (Figure 11A). Hepatic CREB3L3 overexpression significantly increased hepatic *Ppara* and the expression of its target genes (eg, *Cpt1a* and *Fgf21*) in $LDLR^{-/-}$ mice (Figure 11B). Lipogenic genes regulated by SREBP-1c were entirely up-regulated in $LDLR^{-/-}CREB3L3^{-/-}$ mice including fatty acid synthase (*Fasn*), stearoyl-coenzyme A desaturase 1 (*Scd1*), ELOVL family member 6, and elongation of long-chain fatty acids (yeast) (*Elovl6*) (Figure 11A). Another SREBP-1 target, patatin-like phospholipase domain containing 3 (*Pnpla3*), which is a central regulator of hepatic TG metabolism and fat accumulation,[29] was also remarkably increased in $LDLR^{-/-}CREB3L3^{-/-}$ mice (Figure 11A). Notably, in contrast to the marked induction of target genes, the expression of its encoding gene, sterol regulatory element binding transcription factor 1 (*Srebf1*), which is the gene name of SREBP1, was only slightly increased. The expression of cholesterol synthesis genes governed by SREBP-2, such as 3-hydroxy-3-methylglutaryl-CoA synthase 1 (*Hmgcs1*), HMGCoA reductase (*Hmgcr*), and squalene epoxidase (*Sqle*), was increased in $LDLR^{-/-}CREB3L3^{-/-}$ mice, although the encoding gene *Srebf2* did not exhibit apparent changes (Figure 11A). These changes in SREBP-related genes implicate the functional activation of SREBPs at the posttranslational level. In contrast, the expression of *Srebfs* and its target genes per se was not altered between $LDLR^{-/-}$ and $LDLR^{-/-}$TgCREB3L3 mice despite the hepatic overexpression of nuclear, and not full-length, CREB3L3 (Figure 11B).

Interaction Between CREB3L3 and SREBP in Hepatic Lipid Metabolism

To explain that the hepatic expression of lipogenic and cholesterogenic genes was strongly up-regulated in $LDLR^{-/-}CREB3L3^{-/-}$ mice without appreciable induction of *Srebf* expression, we evaluated the proteolytic cleavage of SREBPs by the amount of precursor and nuclear SREBP proteins. Western blotting revealed that the levels of both the premature (membrane; pSREBP-1) and active

(nuclear) forms of SREBP-1 (nSREBP-1), as well as the active form of SREBP-2 (nSREBP-2), were robustly increased in the livers of $LDLR^{-/-}CREB3L3^{-/-}$ mice (Figure 12A). This finding suggests the activated proteocleavage of both proteins and activation of these target genes. SREBPs and CREB3L3 share a set of proteases (S1P and S2P) involved in the cleavage process of transcriptional activation at the Golgi.[3] Thus, the cleavage of these proteins may be competitive to each other. Specifically, we hypothesized that the presence of premature CREB3L3 (pCREB3L3) inhibits the cleavage of pSREBPs in a competitive manner. Accordingly, pCREB3L3 expression was restored in $LDLR^{-/-}CREB3L3^{-/-}$ mice via infection with an adenovirus encoding pCREB3L3 (Ad-pCREB3L3) to determine whether pCREB3L3 could suppress pSREBP cleavage, thus reducing nSREBP accumulation. As expected, pCREB3L3 overexpression reduced nSREBP-1 and nSREBP-2 accumulation in $LDLR^{-/-}CREB3L3^{-/-}$ mice, with only small changes noted in the expression of *Srebfs* (Figure 12B). pCREB3L3 overexpression decreased the plasma TG and TC levels compared with those measured in mice infected with control green fluorescent protein (GFP) (Figure 12B). Genes related to SREBP cleavage were also investigated. An SREBP cleavage activator, *Scap*, was increased in $LDLR^{-/-}CREB3L3^{-/-}$ mice (Figure 12C); this partly explains the activation of SREBP cleavage in $LDLR^{-/-}CREB3L3^{-/-}$ mice. Consistent with a previous report, insulin-induced gene 2a (*Insig2a*), a retention factor of SREBP-SREBF chaperone (SREBP-SCAP) complex in the ER, is a target gene of CREB3L3.[30] *Insig2a* was decreased in $LDLR^{-/-}CREB3L3^{-/-}$ mice (Figure 12C). Other retention factors, such as *Insig1* and *Insig2b*, were not changed in $LDLR^{-/-}CREB3L3^{-/-}$ mice (Figure 12C). Meanwhile, overexpression of nuclear CREB3L3 in $LDLR^{-/-}$ mice failed to affect the expression of *Insig* genes (Figure 12C). This discrepancy between loss and gain of CREB3L3 in $LDLR^{-/-}$ mice indicates that the CREB3L3-INSIG2a pathway is not sufficient to provide an explanation for the strong SREBP activation by CREB3L3 deficiency, supporting the aforementioned new hypothesis. In a cell-based reporter assay using an SREBP response element (SRE)-containing luciferase (SRE-Luc), endogenous SREBP cleavage activity was detected by transfection with pSREBP-1a, an isoform of SREBPs with strong transcriptional activity, as evidenced by SRE-Luc activity (Figure 12D). Further co-transfection with pCREB3L3 significantly suppressed this pSREBP-1a cleavage. However, the active form of CREB3L3 (nCREB3L3) did not (Figure 12D), further supporting the competition in the cleavage between pCREB3L3 and pSREBP.

Antagonism Between CREB3L3 and SREBP Occurs at Trafficking From the ER to the Golgi

An immunoprecipitation assay showed a direct association between the 2 precursor proteins pCREB3L3 and pSREBP-1c (Figure 13A). Further association analysis

exhibited that pCREB3L3 bound to the components related to SREBP-1 translocation from the ER to the Golgi, including INSIG1 and SCAP, respectively (Figure 13B and

C). SCAP is an escort protein of pSREBP-1c for its translocation from the ER to the Golgi, and INSIG1 suppresses the translocation of the SREBP-SCAP complex.[31] The
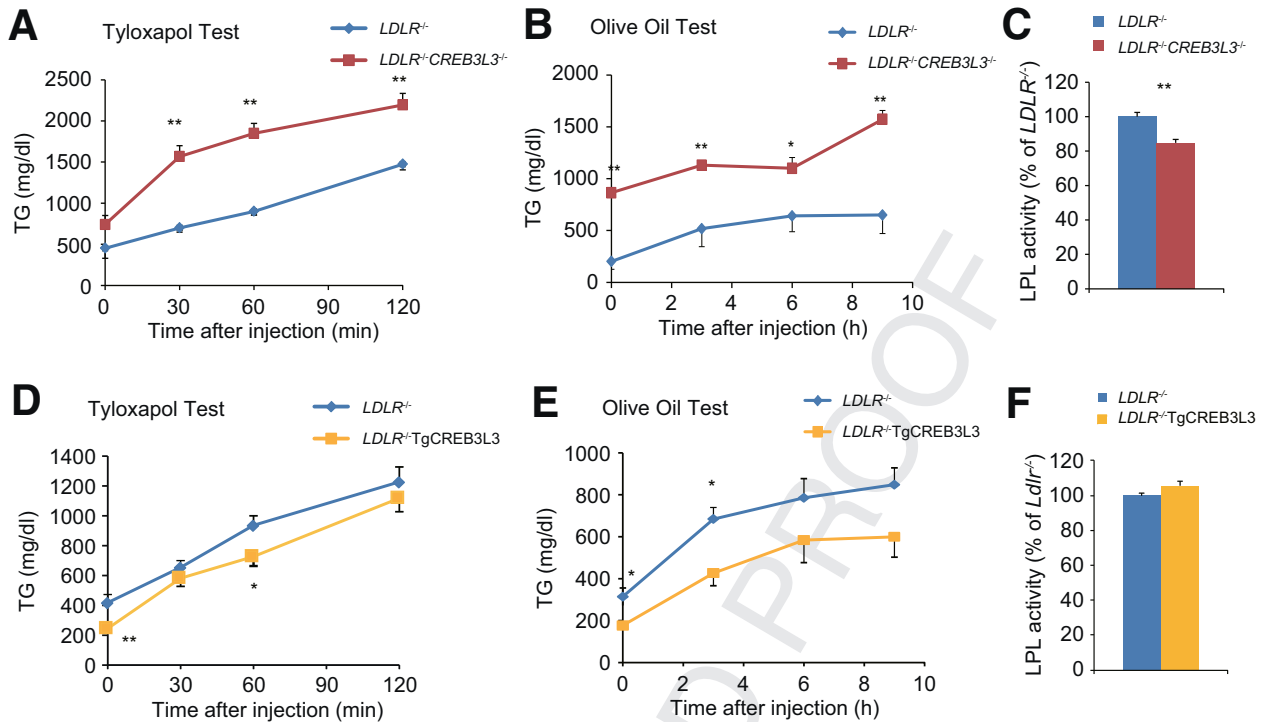
web 4C/FPO
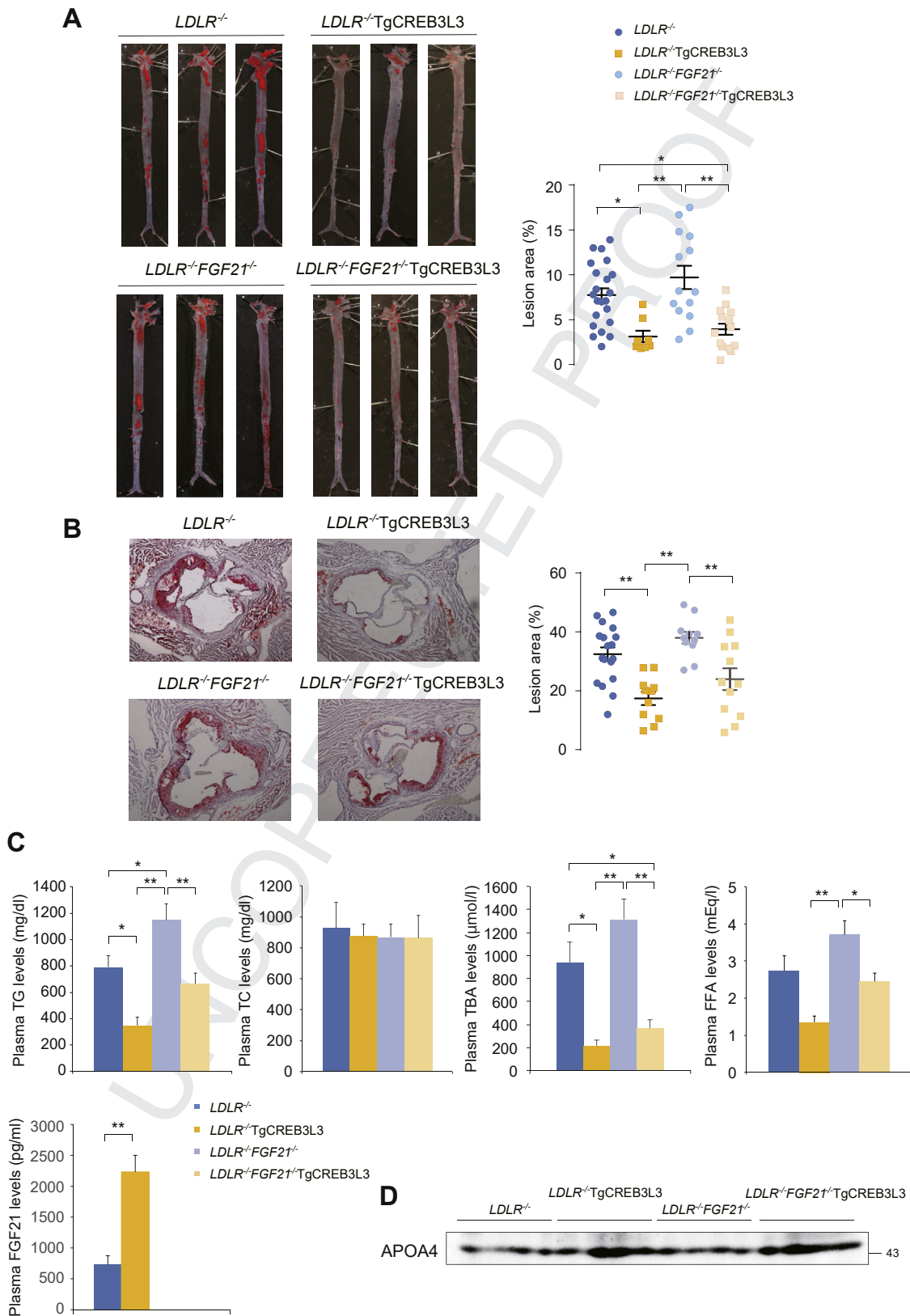
Figure 10. VLDL secretion and TG clearance in $LDLR^{-/-}CREB3L3^{-/-}$ and $LDLR^{-/-}$TgCREB3L3 mice. (*A* and *D*) TG production rates (tyloxapol test) in 8-week-old female $LDLR^{-/-}$ (n = 6) and $LDLR^{-/-}CREB3L3^{-/-}$ (n = 11) mice (*A*) and male $LDLR^{-/-}$ (n = 6) and $LDLR^{-/-}$TgCREB3L3 (n = 6) mice (*D*). Mice were starved for 24 hours and intravenously injected with Triton WR-1339. Plasma was collected at 0, 30, 60, and 120 minutes after injection. **$P < .01$ vs $LDLR^{-/-}$ mice. (*B* and *E*) Postprandial TG responses (olive oil test) in 9-week-old female $LDLR^{-/-}$ (n = 7–8) and $LDLR^{-/-}CREB3L3^{-/-}$ (n = 8) mice (*B*) and male $LDLR^{-/-}$ (n = 7) and $LDLR^{-/-}$TgCREB3L3 (n = 5) mice (*E*). Mice were starved for 16 hours, followed by oral administration of 200 μL olive oil. Plasma was collected at 0, 3, 6, and 9 hours after administration. *$P < .05$ and **$P < .01$ vs $LDLR^{-/-}$ mice. (*C* and *F*) Plasma LPL activity in 8-week-old female $LDLR^{-/-}$ (n = 5) and $LDLR^{-/-}CREB3L3^{-/-}$ mice (n = 6) (*C*) and male $LDLR^{-/-}$ (n = 5) and $LDLR^{-/-}$TgCREB3L3 (n = 5) mice (*F*). *$P < .05$ vs $LDLR^{-/-}$ mice.

pSREBP-1c and SCAP association was increased in a CREB3L3 dose-dependent manner (Figure 13*D*). Similarly, the pSREBP-1 and INSIG1 association was also increased in a CREB3L3 dose-dependent manner (Figure 13*E*). Taken together, pCREB3L3 supports the INSIG1-pSREBP-1c-SCAP complex formation, supporting that pCREB3L3 induces SREBP-1 retention in the ER. To determine the effects of pCREB3L3 on the cellular localization of SREBPs, mCherry-tagged pSREBP-1c and SCAP with or without GFP-tagged pCREB3L3 vectors were co-transfected into HEK293 cells. Immunohistochemistry analysis revealed that SREBP-1c was localized in the nucleus merging with a nuclear marker, 4′,6-diamidino-2-phenylindole (DAPI), when co-transfected with SCAP. This indicated that SCAP enhanced the transport and cleavage of SREBP and caused its nucle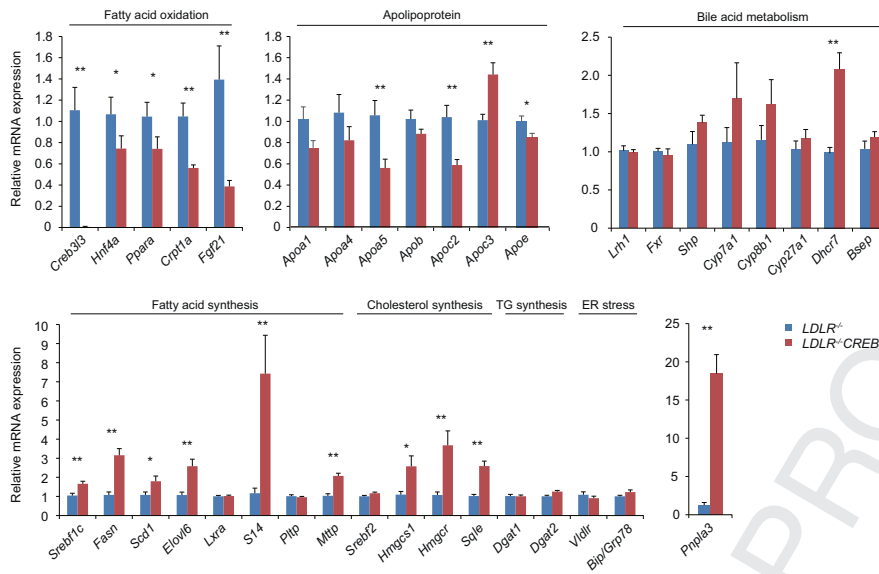ar transfer (Figure 13*F*). However, when also co-transfected with pCREB3L3, SREBP-1c and CREB3L3 were not colocalized in nucleus. This evidence supports the notion that their direct binding leads to the suppression of SREBP cleavage by pCREB3L3 (Figure 13*F*). Organelle marker immunostaining indicated that the colocalization of SREBP-1 and CREB3L3 occurs at the ER because both proteins and the ER marker (calnexin) were merged (Figure 13*G*). The Golgi marker GM130 in SREBP-1c/SCAP transfection showed a partial signal of SREBP-1c merging at the Golgi, presumably a remnant of the uncleaved one and the other partial signal of unmerged one presumably cleaved into the nucleus (Figure 13*H*). SREBP-1c/SCAP/CREB3L3 co-transfection caused only marginal signaling merging of SREBP-1c-CREB3L3 at the Golgi (Figure 13*H*). The data indicate that CREB3L3 inhibited the SCAP escort of SREBP-1c to the Golgi by forming the complex. The

Figure 9. (*See previous page*). **WD for 3 months suppresses development of atherosclerosis in $LDLR^{-/-}$TgCREB3L3 mice.** Ten- to 11-week-old male $LDLR^{-/-}$, $LDLR^{-/-}$TgCREB3L3, $LDLR^{-/-}FGF21^{-/-}$, and $LDLR^{-/-}FGF21^{-/-}$TgCREB3L3 mice were fed a WD for 3 months. Samples were collected in a fed state. (*A*) Representative images of entire Sud IV-stained aortas from $LDLR^{-/-}$ (n = 22), $LDLR^{-/-}$TgCREB3L3 (n = 8), $LDLR^{-/-}FGF21^{-/-}$ (n = 14), and $LDLR^{-/-}FGF21^{-/-}$TgCREB3L3 (n = 14) mice. Surface area occupied by lesions was quantified. *$P < .05$ and **$P < 0.01$ among genotypes. (*B*) Representative aortic root sections from $LDLR^{-/-}$ (n = 18), $LDLR^{-/-}$TgCREB3L3 (n = 11), $LDLR^{-/-}FGF21^{-/-}$ (n = 11), and $LDLR^{-/-}FGF21^{-/-}$TgCREB3L3 (n = 12) mice. Cross sections were stained with Oil Red O and hematoxylin. Aortic root lesion areas were quantified. **$P < .01$ among genotypes. (*C*) Plasma TG, TC, TBA, FFA, and FGF21 levels. n = 6–21; *$P < .05$ and **$P < .01$ among genotypes. (*D*) Plasma APOA4 levels were detected by Western blotting.
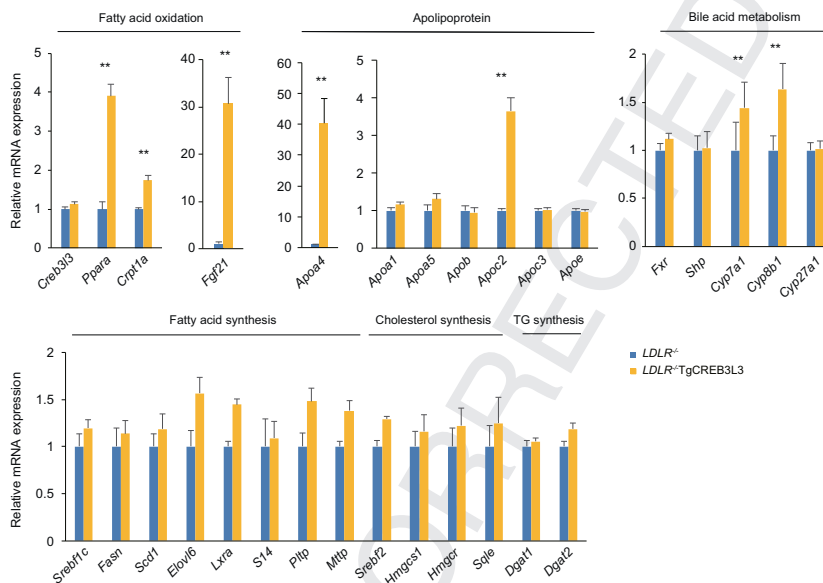
A Liver

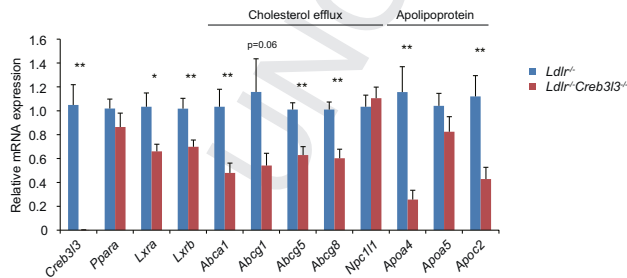**B** Liver

C Intestine

Figure 11. Gene expression in $LDLR^{-/-}$, $LDLR^{-/-}CREB3L3^{-/-}$, **and** $LDLR^{-/-}$ **TgCREB3L3 mice.** Gene expression in livers of 8-week-old female $LDLR^{-/-}$ and $LDLR^{-/-}CREB3L3^{-/-}$ mice (n = 11 per group) (A) and male $LDLR^{-/-}$ and $LDLR^{-/-}$ TgCREB3L3 mice (n = 7 per group) (B) in a fed state with normal diet. *P < .05 and **P < .01 vs $LDLR^{-/-}$ mice. (C) Gene expression in intestines of 8-week-old male $LDLR^{-/-}$ and $LDLR^{-/-}$ TgCREB3L3 mice in a fed state with normal diet (n = 7 per group). *P < .05 and **P < .01 vs $LDLR^{-/-}$ mice.
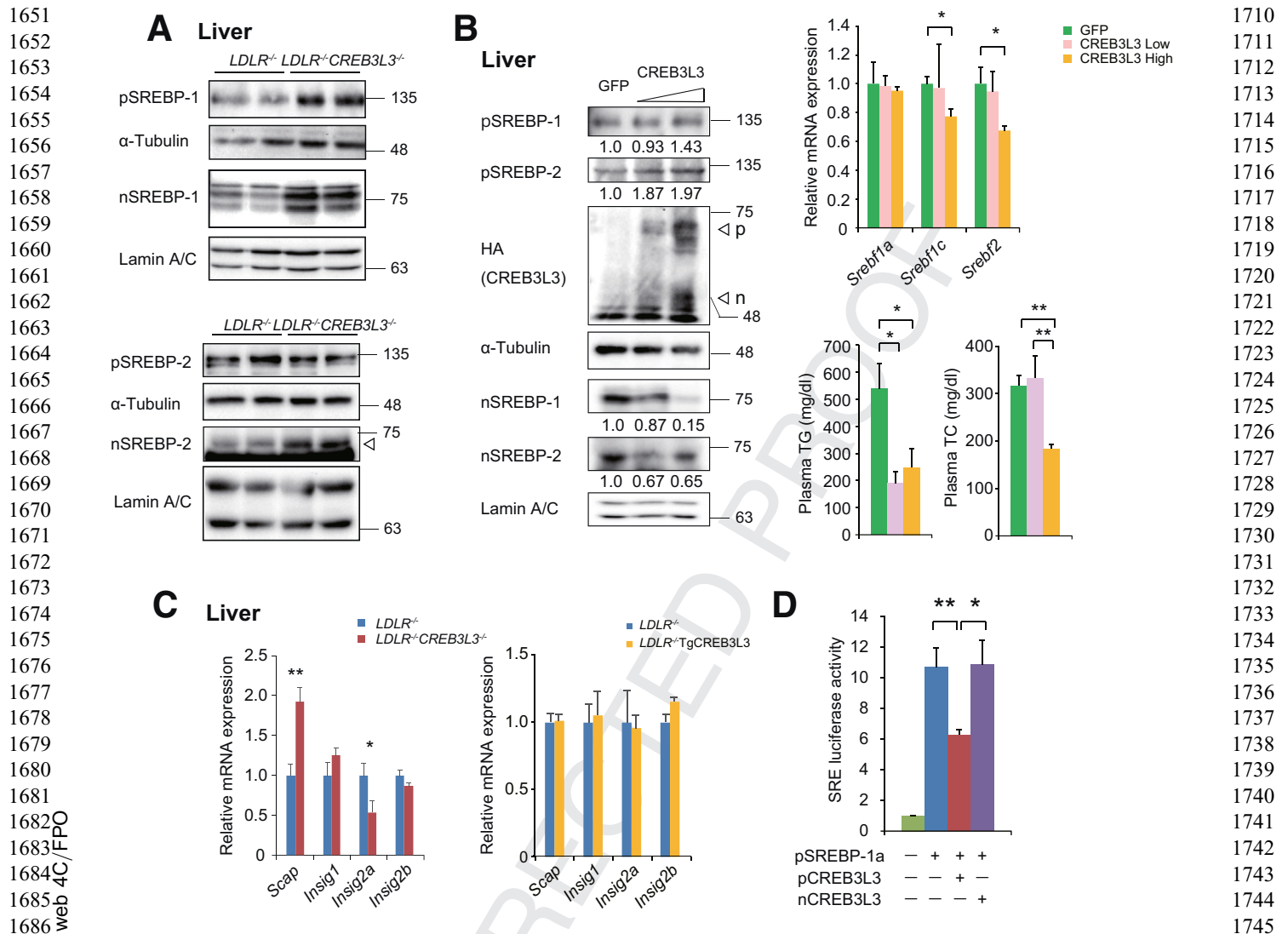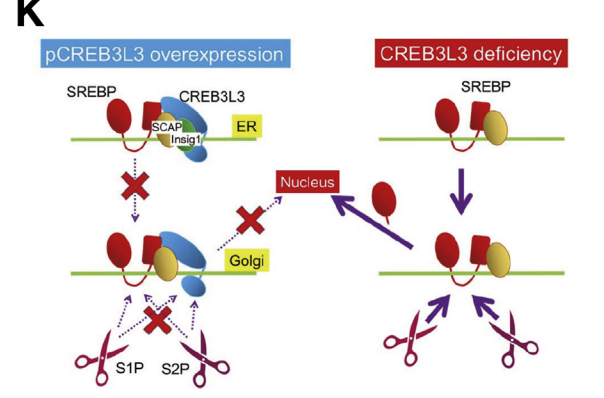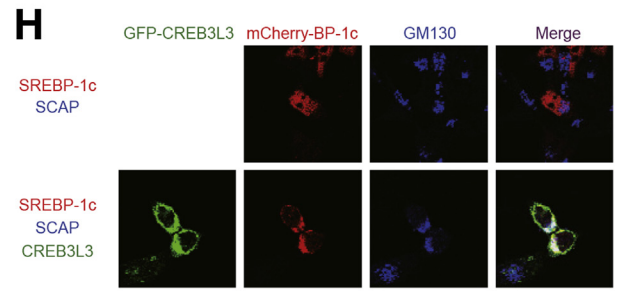
web 4C/FPO

Figure 12. Premature CREB3L3 suppresses cleavage of SREBPs. (*A*) Immunoblotting analysis of SREBPs in hepatic nuclear extracts and total cell lysates from 8-week-old female $LDLR^{-/-}$ and $LDLR^{-/-}CREB3L3^{-/-}$ mice. Each lane was a pooled sample from 3 mouse livers. (*B*) Immunoblotting analysis of SREBPs in hepatic nuclear extracts and total cell lysates. Each lane was a pooled sample from 3 mouse livers. Values were indicated as fold changes of band intensity versus GFP infection, hepatic expression of *Srebfs*, and plasma TG and TC levels in 10-week-ol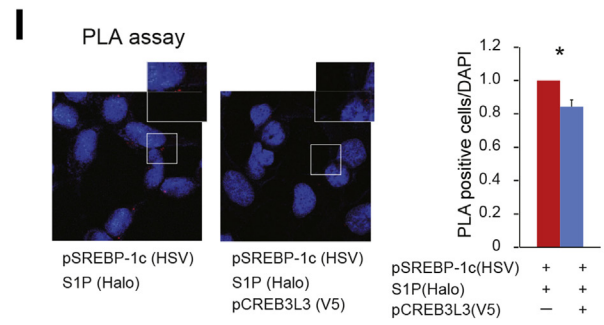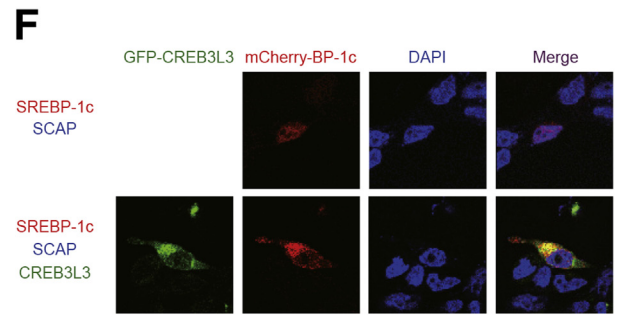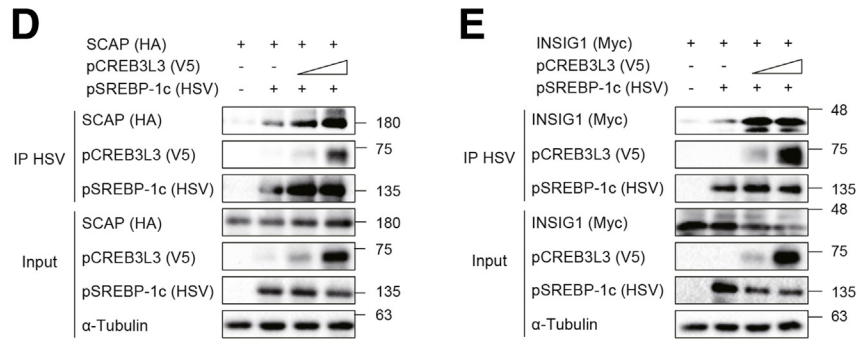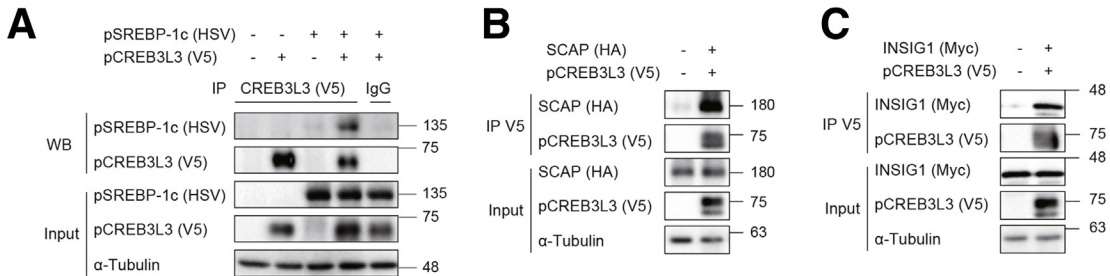d female $LDLR^{-/-}$ and $LDLR^{-/-}CREB3L3^{-/-}$ mice infected with adenoviruses encoding GFP and the low and high dose of full-length CREB3L3 (pCREB3L3) after feeding with normal diet for 6 days. n = 4–8. *$P < .05$ and **$P < .01$ vs $LDLR^{-/-}$ mice. (*C*) Hepatic SREBP cleavage modulator gene expression in 8-week-old female $LDLR^{-/-}$ and $LDLR^{-/-}CREB3L3^{-/-}$ and 8-week-old male $LDLR^{-/-}$ and $LDLR^{-/-}$ TgCREB3L3 mice in a fed state with normal diet. n = 4–6. *$P < .05$ and **$P < .01$ vs $LDLR^{-/-}$ mice. (*D*) pCREB3L3 suppresses SREBP transcriptional activity. pCREB3L3 or the active form of CREB3L3 (mCREB3L3) and pSREBP expression vectors were co-transfected with an SRE-luc vector into HEK293 cells. Luciferase activity was determined after 48 hours. n = 4–8. *$P < .05$ and **$P < .01$ vs Control.

complex remained in the ER, thus not allowing the entry of SREBP-1c to the Golgi. To further investigate whether pCREB3L3 disrupts the pSREBPs-S1P complex, we used an in situ microscopy approach through a proximity ligation assay (PLA). Herpes simplex virus (HSV)–tagged pSREBP-1c and Halo-tagged S1P were co-transfected into HEK293 cells. Complexes between pSREBP-1c and S1P were observed as red dots around the nucleus (Figure 13*I*). As CREB3L3 inhibited its complex formation, the red dots were significantly decreased in addition to pCREB3L3 transfection (Figure 13*I*). This indicates that pCREB3L3

inhibited the formation of the complex between pSREBP-1c and S1P. These findings suggest that the physical association of CREB3L3 with SREBPs inhibits the SCAP-mediated transport of SREBP-1 from the ER to the Golgi, the processing by S1P, and, consequently, SREBP transcriptional activity. To verify this observation vice versa (ie, whether CREB3L3 cleavage is conversely inhibited by SREBP), we evaluated the nCREB3L3 protein levels in $SREBF1^{-/-}$ mice. Hepatic nCREB3L3 protein levels in $SREBF1^{-/-}$ mice were clearly increased compared with those measured in wild-type mice (Figure 13*J*). These

web 4C/FPO

results support that CREB3L3 and SREBP-1 can antagonize each other through direct mutual interaction at the precursor protein level.

Discussion

The present study clearly exhibited that CREB3L3 profoundly impacts the atherosclerotic phenotypes. *CREB3L3* deletion caused both hypertriglyceridemia and hypercholesterolemia and accelerated aortic atheroma formation in $LDLR^{-/-}$ mice fed either a WD or a normal diet, irrespective of sex, and from both hepatic and intestinal origins. Conversely, hepatic nuclear CREB3L3 overexpression strikingly attenuated WD-induced hyperlipidemia and atherosclerosis progression in $LDLR^{-/-}$ mice. Numerous studies, as well as the present work, confirmed that the primary role of CREB3L3 is the regulation of TG metabolism.[1,14,24,32,33] TG has been proposed as the major atherosclerosis risk factor, highlighting the potential cholesterol-related or more comprehensive mechanisms of the anti-atherogenic effects of CREB3L3.

In the process of clarifying the causative mediators of the anti-atherogenic effect of CREB3L3, FGF21 (a major hepatic CREB3L3 target gene that regulates both lipid and glucose metabolism) had been a strong candidate. It has been reported that FGF21 ameliorates atherosclerosis and leads to the hepatic activation of SREBP-2 in $APOE^{-/-}FGF21^{-/-}$ mice.[16,34] Although the present study also showed that some metabolic phenotypes observed in $LDLR^{-/-}CREB3L3^{-/-}$ mice were attributed to decreases in plasma FGF21 levels, deficiency of *FGF21* in $LDLR^{-/-}$TgCREB3L3 mice did not cancel the improvement in atherosclerosis, distracting the hypothesis that FGF21 is the main contributor to anti-atherosclerosis.

The IKO mice also exhibited atheroma formation, which was comparable to that noted in LKO mice, confirming the role of intestinal CREB3L3 in anti-atherogenic action. Consistent with previous report that CREB3L3 controls LXR acitivity,[35] decreased LXR signaling and increased lipid contents were observed in the intestines of $LDLR^{-/-}CREB3L3^{-/-}$ mice. Overexpression of the intestinal-specific active form of LXR in $LDLR^{-/-}$ mice on a WD increased fecal neutral sterol excretion and exhibited protection against atherosclerosis.[28] These results support the hypothesis that intestinal CREB3L3 contributes to cholesterol metabolism via LXR. $LDLR^{-/-}CREB3L3^{-/-}$ mice had higher plasma plant sterol levels than $LDLR^{-/-}$ mice, explaining that *CREB3L3* deficiency in the small intestines increases cholesterol absorption. Collectively, the data suggest that both liver- and intestine-specific CREB3L3 deficiency additively promote atherosclerosis.

We showed that *CREB3L3* deficiency increases the levels of hepatic nSREBPs and, consequently, plasma lipids. This led us to speculate and confirm the two-step CREBH-mediated suppression of SREBP-1c activation: (1) CREB3L3 induces the retention of SPREBP-1c in the ER by promoting the formation of the CREB3L3/INSIG1/SCAP/SREBP complex, and (2) CREB3L3 physically competes with SREBPs for cleavage by S1P and S2P in the Golgi. Therefore, CREB3L3 deletion may result in primarily decreased TG catabolism and enhanced lipogenesis as a secondary consequence of SREBP-1c activation, leading to a marked accumulation of TG-rich remnant lipoproteins and severe hypertriglyceridemia. In addition, both increased cholesterol absorption due to the absence of intestinal CREB3L3 and cholesterol synthesis mediated by SREBP-2 activation in the liver significantly enriched these lipoproteins with cholesterol and played a major role in the production of more atherogenic lipoproteins.

Functional competition between SREBPs and CREB3L3 implicates profound physiological consequences for lipid and energy regulation. CREB3L3 and SREBPs use the same activation process of intramembrane proteolysis regulation. Through this process, transmembrane proteins are cleaved to release cytosolic domains that translocate into the nucleus and thereby regulate gene transcription. CREB3L3 is cleaved by the processing enzymes S1P and S2P in the Golgi apparatus in a manner similar to that of SREBP cleavage.[3] Therefore, we initially hypothesized that pCREB3L3 would competitively inhibit SREBP processing. We showed that CREB3L3, SREBP-1c, and INSIG1 physically interact (Figure 13E), possibly to inhibit the trafficking of the SREBP-INSIG1-CREB3L3 complex from the ER to the Golgi. Recently, it was reported that CREB3L3 increases *Insig2a* expression, which in turn suppresses SREBP activation.[30] Consistently, its expression was decreased in the livers of $LDLR^{-/-}CREB3L3^{-/-}$ mice but not changed in those of $LDLR^{-/-}$TgCREB3L3 mice. In addition, $LDLR^{-/-}$TgCREB3L3 mice (overexpressing nCREB3L3) did not exhibit apparently altered SREBPs and activation of their target genes in the liver. Certainly, adenoviral overexpression of pCREB3L3 in the livers of $LDLR^{-/-}CREB3L3^{-/-}$ mice reduced the expression of nSREBP-1 and nSEEBP-2 proteins (Figure 12B). This result indicated that in $LDLR^{-/-}$ mice, SREBP cleavage was regulated by the existence of pCREB3L3 rather than INSIGs. It was previously reported that CREB3L3 suppresses LXRα-induced *Srebf1c* expression by inhibiting LXRα binding to the *Srebf1c* promoter.[36]

Figure 13. (*See previous page*). **Premature CREB3L3 associates with SREBP and SREBP transport regulatory proteins.** (A–E) Physical association among CREB3L3, SREBP, and SREBP transport regulatory proteins. Indicated vectors were co-transfected into HEK293 cells. After 24 hours, cell lysates were collected and immunoprecipitated with an anti-V5 antibody. Immunoprecipitants were detected with the indicated antibodies. (F–H) Localization of SREBP-1c and CREB3L3 in the cellular component. mCherry-pSREBP-1c (mCherry-BP-1c) and SREBF chaperone (SCAP), with/without GFP-pCREB3L3 (GFP-CREB3L3), were co-transfected into HEK293 cells. 4′,6-diamidino-2-phenylindole (DAPI) for the nucleus (F), calnexin for ER (G), and GM130 for the Golgi apparatus (H) were immunostained. (I) CREB3L3 inhibits SREBPs-S1P interaction. Using the DuoLink PLA, *red dots* showed the pSREBP-1c-S1P association. *P < .05. (J) Immunoblot analysis of CREB3L3 in hepatic nuclear extracts and total cell lysates from 16-week-old male wild-type (WT) and $SREBF1^{-/-}$ mice. (K) Schematic representation of atherosclerosis development via a competitive transport interaction of SREBPs and CREB3L3.

Table 1. Primers Used for Real-Time Polymerase Chain Reaction Analysis

Gene name	Forward	Reverse
Abca1	AAAACCGCAGACATCCTTCAG	CATACCGAAACTCGTTCACCC
Abcg1	CCATGAATGCCAGCAGCTACT	CTGTGAAGTTGTTGTCCACCTTCT
Abcg5	AGGGCCTCACATCAACAGAG	GCTGACGCTGTAGGACACAT
Abcg8	AGTGGTCAGTCCAACACTCTG	GAGACCTCCAGGGTATCTTGAA
Acox1	CGATCCAGACTTCCAACATGAG	CCATGGTGGCACTCTTCTTAACA
Angptl3	TCTACTGTGATACCCAATCAGGC	CATGTTTCGTTGAAGTCCTGTGA
Angptl4	GCATCCTGGGACGAGATGAAC	CCCTGACAAGCGTTACCACA
Angptl6	TTGGGCGTCCAGAAGGAGAA	CAGTCCTCTAGGAGTATCAGCAG
Apoa1	TCACCCACACCCTTCAGGAT	CTGGCTCCCTGTCAGGAAGA
Apoa4	TTACCCAGCTAAGCAACAATGC	GAGGGTACTGAGCTGCTGAGTGA
Apoa5	GCGAGTTCTGCCGTAGGAC	CCCAACCCCATCAAATGTGA
Apob	TTGGCAAACTGCATAGCATCC	TCAAATTGGGACTCTCCTTTAGC
Apoc2	CCAAGGAGGTTGCCAAAGAC	TGCCTGCGTAAGTGCTCATG
Apoc3	TACAGGGCTACATGGAACAAGC	CAGGGATCTGAAGTGATTGTCC
Bip	ACATCAAGCAGTACCAGATCAC	AACCCCGATGAGGCTGTAGC
Bsep	CAATGTTCAGTTCCTCCGTTCA	TCTCTTTGGTGTTGTCCCCATA
Cpt1a	CCTGGGCATGATTGCAAAG	GGACGCCACTCACGATGTT
Creb3l3	CCTGTTTGATCGGCAGGAC	CGGGGGACCATAATGGAGA
Cyclophilin	TGGCTCACAGTTCTTCATAACCA	ATGACATCCTTCAGTGGCTTGTC
Cyp7a1	GCTGAGAGCTTGAAGCACAAGA	TTGAGATGCCCAGAGGATCAC
Cyp8b1	CTAGGGCCTAAAGGTTCGAGT	GTAGCCGAATAAGCTCAGGAAG
Cyp27a1	CCAGGCACAGGAGAGTACG	GGGCAAGTGCAGCACATAG
Dhcr7	CACCGGCCGTGCTAGTCTGG	CAGGCTTGTAGCCCGTTCACCTC
Dgat1	CGTGGGCGACGGCTACT	GAAACCACTGTCTGAGCTGAACA
Dgat2	GCCCGCAGCGAAAACA	GTCTTGGAGGGCTGAGAGGAT
Elovl6	ACAATGGACCTGTCAGCAAA	CTACCAGTGCAGGAAGATCAGT
Fasn	ATCCTGGAACGACGAGAACACGATCT	AGAGACGTGTCATCCTGGACTT
Fbwx7a	CTCACCAGCTCTCCTCTCCATT	GCTGAACATGGTACAAGGCCA
Fgf21	AGATCAGGGAGGATGGAACA	TCAAAGTGAGGCGATCCATA
Fxr	CTCTGCTCACAGCGATCGTC	CACCGCCTCTCTGTCCTTGA
Hmgcs1	AACTGGTGCAGAAATCTCTAGC	GGTTGAATAGCTCAGAACTAGCC
Hmgcr	GAGAAGAAGCCTGCTGCATA	CGTCAACCATAGCTTCCGTAGTT
Insig1	TCACAGTGACTGAGCTTCAGCA	TCATCTTCATCACACCCAGGAC
Insig2a	CCCTCAATGAATGTACTGAAGGATT	TGTGAAGTGAAGCAGACCAATGT
Insig2b	CCGGGCAGAGCTCAGGAT	GAAGCAGACCAATGTTTCAATGG
Lxra	AGCAACAGTGTAACAGGCGCT	ACGATGGCCAGCTCAGTAAAGT
Lxrb	ATGTCTTCCCCCACAAGTTCT	GACCACGATGTAGGCAGAGC
Mttp	AGCTTTGTCACCGCTGTGC	TCCTGCTATGGTTTGTTGGAAGT
Npc1l1	ATCCTCATCCTGGGCTTTGC	GCAAGGTGATCAGGAGGTTGA
Pltp	GACGACGAGAGGATGGTGTACG	GTCGGACTCAGGAGAACAATGC
Pnpla3	TCACCTTCGTGTGCAGTCTC	CCTGGAGCCCGTCTCTGAT
Ppara	TTGTGGCTGGTCAAGTTCGG	GCTCTCTGTGTCCACCATGT
S14	ATGCAAGTGCTAACGAAACGC	GGAGTACCGATCCATGACTGTC
Scap	ATTTGCTCACCGTGGAGATGTT	GAAGTCATCCAGGCCACTACTAATG
Scd1	AGATCTCCAGTTCTTACACGACCAC	CTTTCATTTCAGGACGGATGTCT
Shp	CAAGGAGTATGCGTACCTGAAG	CCTGGCACATCTGGGTTGAAG
Sqle	AAATCAGAGCCGTGGGCTAC	GGAAGTGACACAGTTCTATG
Srebf1c	CGGCGCGGAAGCTGT	TGCAATCCATGGCTCCGT
Srebf2	CTGCAGCCTCAAGTGCAAAG	CAGTGTGCCATTGGCTGTCT
Vldlr	TTCCTAGCTCATCCTCTTGCAC	CTGACCCAGTGAATTTATTGGC

However, our data did not show changes in *SREBF1c* and its target genes in *LDLR*$^{-/-}$TgCREB3L3 mice.

We propose the new concept that CREB3L3, SREBPs, and INSIG1 physically interact at the ER, inhibiting the transportation of SREBPs to the Golgi apparatus, and CREB3L3 competes with SREBPs in access to S1P in the Golgi apparatus. Loss of this interaction because of CREB3L3 deficiency induces SREBP-1 and -2 cleavage and promotes the induction of TG and cholesterol synthesis (Figure 13K). This mechanism also explains why the overexpression of nuclear CREB3L3 did not suppress hepatic SREBP target genes (Figure 11B), because nuclear CREB3L3 does not compete with pSREBPs. In the normal liver, *Creb3l3* is up-regulated during fasting and down-regulated under feeding conditions; *Srebf1c* is regulated in a reciprocal manner. Thus, the encounter of the 2 factors does not actively occur on the ER under normal nutritional states. However, in metabolic disturbances with high atherogenic risks, such as *db/db* or *ob/ob* mice, these 2 factors could be expressed collaterally[14] and interact with and inhibit each other. Finally, enhancement of nCREB3L3 with decreased pCREB3L3 in the *SREBF1*$^{-/-}$ liver (Figure 13J) supports this hypothesis. Functional antagonism between CREB3L3 and SREBPs in atherosclerosis is consistent on the basis of the anti-atherogenic action of CREB3L3 from the current data and pro-atherogenic action of SREBP-1 from our previous work.[37] CREB3L3 and SREBPs are regulators of the catabolism and anabolism of lipids, respectively. Hence, it is conceivable to configure a mechanism by which mutual interaction and balance of the counterpartners maintain the whole-body energy balance and atherosclerosis risks.

Conclusions

Collectively, our study is the first to identify the crucial role of CREB3L3 enterohepatic interplay in lipid metabolism and prevention of atherosclerosis. Therefore, CREB3L3 may be a new target against atherosclerosis. Protection from atherosclerosis by overexpression of nuclear CREB3L3 in mice was greater than that expected from the amelioration of hyperlipidemia in *LDLR*$^{-/-}$TgCREB3L3 mice. CREB3L3 is deeply involved in cellular stress and inflammation, which we have not investigated in the present study. Therefore, further study is warranted to address these aspects.

Methods
Mice

This project was approved by and conducted under the guidelines of the Animal Care Committee of the University of Tsukuba. *CREB3L3*$^{tm1.1Sad/J}$ (*CREB3L3*$^{-/-}$) mice[5] and *LDLR*$^{-/-}$ mice[38] were purchased from the Jackson Laboratory (Bar Harbor, ME). *CREB3L3*$^{-/-}$ mice were crossed onto an *LDLR*$^{-/-}$ background to generate *LDLR*$^{-/-}$*CREB3L3*$^{-/-}$ mice. Tg mice overexpressing amino acids 1–320 of human CREB3L3 under control of the phosphoenolpyruvate carboxykinase promoter on the C57BL/6J background (hereafter referred to as TgCREB3L3) were generated as previously described.[14] *FGF21*$^{-/-}$ mice were provided by Professors Morichika Konishi and Nobuyuki Ito.[39]

TgCREB3L3 mice were crossed with *LDLR*$^{-/-}$ mice to produce *LDLR*$^{-/-}$TgCREB3L3 mice and subsequently crossed with *FGF21*$^{-/-}$ mice to produce *LDLR*$^{-/-}$*FGF21*$^{-/-}$ TgCREB3L3 mice. *CREB3L3*$^{flox/flox}$ (flox) mice were generated using the CRISPR/Cas 9 system as previously described.[24] Flox mice were crossed with B6.Cg-Tg(Alb-Cre) 21Mgn/J (albumin Cre Tg; Jackson Laboratory)[40] and/or villin Cre Tg mice (Jackson Laboratory)[41] to produce LKO, IKO, and DKO mice. These mice were crossed with *LDLR*$^{-/-}$ mice, generating *LDLR*$^{-/-}$flox, *LDLR*$^{-/-}$LKO, *LDLR*$^{-/-}$IKO, and *LDLR*$^{-/-}$DKO mice, respectively. *SREBF1*$^{-/-}$ mice were generated as previously described.[42] Sixteen-week-old male wild-type and *SREBF1*$^{-/-}$ mice were fasted for 24 hours and fed with high-sucrose diet for 12 hours.[43] All mice were maintained on normal diet (Oriental Yeast Company, Tokyo, Japan) and a 14-hour light/10-hour dark cycle. For the atherosclerosis analyses, mice were fed a WD (D12079B [34% sucrose, 21% fat, 0.15% cholesterol]; Research Diets, Inc, New Brunswick, NJ) under the indicated conditions.[37] For adenoviral infection, 8- to 10-week-old female *LDLR*$^{-/-}$ *CREB3L3*$^{-/-}$ mice were infected with the indicated adenovirus at 1.0 (low) and 5.0 (high dose) $\times$ 10^8 plaque-forming units/g body weight; samples were collected 6 days later while in a fed state. All animal husbandry procedures and animal experiments were consistent with the University of Tsukuba Regulations of Animal Experiment and approved by the Animal Experiment Committee of the University of Tsukuba.

Determination of Metabolic Parameters

Plasma levels of glucose, TGs, TC, TBA, FFA, alanine aminotransferase, and aspartate aminotransferase were measured using Wako enzymatic kits (Wako Pure Chemical Industries, Osaka, Japan). Plasma insulin was measured with a mouse insulin enzyme-linked immunosorbent assay (ELISA) kit (Sibayagi, Gunma, Japan). Plasma FGF21 was measured with a mouse/rat FGF21 Quantikine ELISA kit (R&D Systems, Minneapolis, MN). Hepatic TG, TC, and TBA contents were measured as previously described.[23,43] Intestinal TG and TC contents were measured using the same protocol. Plasma APOA4 was detected by Western blotting with an anti-APOA4 antibody (sc-19036; Santa Cruz Biotechnology, Santa Cruz, CA).

HPLC Analysis

For the lipoprotein distribution analysis, pooled plasma samples from 4 or 5 mice per group were analyzed via upgraded HPLC analysis, as previously described (Skylight Biotech Inc, Tokyo, Japan).[44]

Isolation of the VLDL Fraction

VLDL (d < 1.006 g/mL) was isolated via ultracentrifugation with a TLA120.2 rotor (Beckman Coulter, Brea, CA). VLDL fractions were separated by sodium dodecyl sulfate–polyacrylamide gel electrophoresis and subjected to Coomassie brilliant blue staining.

Determination of Plasma Sterol Levels

For the sterol distribution analysis, pooled plasma samples were quantified by using a gas chromatography method (Skylight Biotech Inc).

Immunoblotting

Total cell and nuclear fraction lysates were prepared as previously described[45] and separated by sodium dodecyl sulfate–polyacrylamide gel electrophoresis. Subsequently, the samples were subjected to Western blotting analysis using antibodies against SREBP-1 (sc-12332; Santa Cruz Biotechnology), SREBP-2 (10007663; Cayman Chemical, Ann Arbor, MI), α-tubulin (05-829; Millipore, Burlington, MA), lamin A/C (#2032; Cell Signaling Technology, Danvers, MA), V5 (R960; Life Technologies, Carlsbad, CA), HSV (69171-3; Novagen, Millipore), MYC (9E10; Santa Cruz Biotechnology), and hemagglutinin (3F10; Roche, Basel, Switzerland) antibodies.

Immunoprecipitation

HEK293 cells were maintained in Dulbecco modified Eagle medium supplemented with 10% fetal bovine serum and penicillin/streptomycin. Indicated plasmids were transfected with X-tremeGENE 9 (Roche) according to the instructions provided by the manufacturer. V5-tagged full-length mouse *CREB3L3* cDNA was inserted into pcDNA3.1 (Invitrogen, Carlsbad, CA); GFP-tagged full-length mouse *CREB3L3* cDNA was inserted into pEGFP (GFP-CREB3L3) (Clontech, Mountain View, CA); mCherry-tagged human SREBP-1c was inserted into pmCherry (mCherry-SREBP-1c) (Clontech); and hemagglutinin-tagged hamster SCAP, Myc-tagged mouse INSIG1, HSV-tagged human SREBP-1c, and HSV-tagged human SREBP-2 were inserted into pCMV. Cell lysates were immunoprecipitated with antibodies against V5, and immunoprecipitants were subjected to immuno-blotting with the indicated antibodies as previously described.[14]

Duolink PLA

HEK293 cells were co-transfected with HSV-tagged pSREBP-1c and Halo-tagged S1P with/without pCREB3L3. Cells were fixed with 3.7% formalin in phosphate-buffered saline for 30 minutes before being permeabilized with 0.2% Triton X-100 in phosphate-buffered saline for 10 minutes. Cells were subsequently subjected to the PLA using the Duolink red kit (Sigma–Aldrich, St Louis, MO) according to the instructions provided by the manufacturer.

Immunocytochemistry

HEK293 cells were transfected with mCherry-tagged pSREBP-1c, SCAP, and GFP-tagged pCREB3L3 using X-tremeGENE 9 (Roche). Cells were grown on coverslips, fixed with 4% paraformaldehyde for 15 minutes, and per-meabilized with 0.1% Triton X-100 for 5 minutes. After blocking in 1% bovine serum albumin for 30 minutes, the cells were incubated with primary and secondary antibodies for 1 hour each. The ER and Golgi apparatus were stained using anti-calnexin (610523; BD Biosciences, San Jose, CA) and anti-GM130 antibodies (610822; BD Biosciences), respectively. Immunoreactive complexes were visualized with Alexa Fluor 405-conjugated secondary antibody (ab175660; Abcam, Cambridge, UK), and nuclei were visu-alized by staining with DAPI.

Promoter Analysis

HEK293 cells were transfected with the indicated lucif-erase reporter, expression plasmids, and a reference pRL-SV40 plasmid (Promega, Madison, WI) using X-tremeGENE 9 (Roche). SRE-luc vector[45–47] and human SREBP-1a[45,46] have been previously described. After a 48-hour incubation, firefly luciferase activity in cells was measured and normalized to *Renilla* luciferase activity.

Atherosclerotic Lesion Analysis

Ten- to 11-week-old male and female $LDLR^{-/-}$ and $LDLR^{-/-}CREB3L3^{-/-}$ mice (age 10–11 weeks) were fed a WD containing 34% sucrose, 21% fat, and 0.15% choles-terol (D12079B; Research Diets, Inc) for 5 weeks or 3 months. Ten- to 11-week-old male $LDLR^{-/-}$ and $LDLR^{-/-}$TgCREB3L3 mice (age 10–11 weeks) were fed a WD for 3 months. The mice were subsequently euthanized to extract their hearts and aortas. Hearts were fixed in 4% formalin for >48 hours. The basal half of each heart was embedded in Tissue-Tek OCT compound (Sakura Finetek, Torrance, CA). Cross sections were stained with Oil Red O and he-matoxylin. Aortas were cut along the midline from the iliac arteries to the aortic root, pinned flat, and treated with Sudan IV for 15 minutes to stain lesions, followed by 70% ethanol destaining and fixation in 4% phosphate-buffered formalin.[37] Atherosclerotic lesions were quantified using the Photoshop CS software (Adobe Systems Inc, San Jose, CA).

TG Production

Mice were deprived of food for 24 hours and subse-quently injected with Triton WR-1339 (0.5 mg/g body weight; Sigma–Aldrich) via the tail veins to block the clearance of nascent APOB-containing lipoproteins. Blood samples were collected at 0, 30, 60, and 120 minutes after injection.[37]

Postprandial TG Response

Mice were deprived of food for 16 hours, followed by oral administration of 200 μL olive oil.[1] Blood samples were collected at 0, 3, 6, and 9 hours after administration.

Intestinal TG Absorption

Mice were fasted for 3 hours and injected with Triton WR-1339 (1 mg/g body weight; Sigma–Aldrich) via the tail veins. After injection (2 hours), mice received 100 μL olive oil orally.[48] Blood samples were collected for up to 3 hours after the injection.

Determination of Plasma LPL Activity

Mice were injected with 100 U/kg body weight of heparin (Novo Heparin; Mochida Pharmaceutical Co, Ltd, Tokyo, Japan) via the tail veins. Blood samples were collected at 20 minutes after administration. Plasma LPL activity was determined by using an LPL activity assay kit (Roar Biochemical, Inc, Huntington, NY) according to the instructions provided by the manufacturer.

Preparation of Recombinant Adenovirus

cDNAs encoding human full-length of CREB3L3 (NM_032607.2) and GFP were cloned into pENTR4 vectors (Life Technologies). In addition, adenovirus vectors were recombined with pAd/CMV/V5-DEST vectors (Life Technologies). Recombinant adenoviruses were produced in 293A cells (Invitrogen) and purified via cesium chloride gradient centrifugation, as previously described.[43]

Analysis of Gene Expression

Total RNA was isolated from cells and tissues using Trizol reagent (Invitrogen) and Sepasol (Nacalai, Kyoto, Japan). Real-time polymerase chain reaction analysis templates were prepared via cDNA synthesis (Invitrogen) from total RNA. Real-time polymerase chain reaction was performed using the ABI Prism 7300 System (Applied Biosystems, Inc, Foster City, CA) with SYBR Green Master Mix (Roche) and TB Green Premix EX Taq II (TAKARA Bio, Shiga, Japan).[49] Primer sequences are described in Table 1.

Statistical Analysis

Statistical significance was determined by using unpaired Student *t* tests and one-way analysis of variance with Tukey's post hoc using the GraphPad Prism software (San Diego, CA). Differences with *P* values <.05 were considered significant. Data are expressed as the mean ± standard error of the mean.

References

1. Lee JH, Giannikopoulos P, Duncan SA, Wang J, Johansen CT, Brown JD, Plutzky J, Hegele RA, Glimcher LH, Lee AH. The transcription factor cyclic AMP-responsive element-binding protein H regulates triglyceride metabolism. Nat Med 2011;17:812–815.

2. Omori Y, Imai J, Watanabe M, Komatsu T, Suzuki Y, Kataoka K, Watanabe S, Tanigami A, Sugano S. CREB-H: a novel mammalian transcription factor belonging to the CREB/ATF family and functioning via the box-B element with a liver-specific expression. Nucleic Acids Res 2001;29:2154–2162.

3. Zhang K, Shen X, Wu J, Sakaki K, Saunders T, Rutkowski DT, Back SH, Kaufman RJ. Endoplasmic reticulum stress activates cleavage of CREBH to induce a systemic inflammatory response. Cell 2006; 124:587–599.

4. Danno H, Ishii KA, Nakagawa Y, Mikami M, Yamamoto T, Yabe S, Furusawa M, Kumadaki S, Watanabe K, Shimizu H, Matsuzaka T, Kobayashi K, Takahashi A, Yatoh S, Suzuki H, Yamada N, Shimano H. The liver-enriched transcription factor CREBH is nutritionally regulated and activated by fatty acids and PPARalpha. Biochem Biophys Res Commun 2010; 391:1222–1227.

5. Luebke-Wheeler J, Zhang K, Battle M, Si-Tayeb K, Garrison W, Chhinder S, Li J, Kaufman RJ, Duncan SA. Hepatocyte nuclear factor 4alpha is implicated in endoplasmic reticulum stress-induced acute phase response by regulating expression of cyclic adenosine monophosphate responsive element binding protein H. Hepatology 2008;48:1242–1250.

6. Steinmetz A, Utermann G. Activation of lecithin: cholesterol acyltransferase by human apolipoprotein A-IV. J Biol Chem 1985;260:2258–2264.

7. Chen CH, Albers JJ. Activation of lecithin: cholesterol acyltransferase by apolipoproteins E-2, E-3, and A-IV isolated from human plasma. Biochim Biophys Acta 1985;836:279–285.

8. Fournier N, Atger V, Paul JL, Sturm M, Duverger N, Rothblat GH, Moatti N. Human ApoA-IV overexpression in transgenic mice induces cAMP-stimulated cholesterol efflux from J774 macrophages to whole serum. Arterioscler Thromb Vasc Biol 2000;20:1283–1292.

9. Steinmetz A, Barbaras R, Ghalim N, Clavey V, Fruchart JC, Ailhaud G. Human apolipoprotein A-IV binds to apolipoprotein A-I/A-II receptor sites and promotes cholesterol efflux from adipose cells. J Biol Chem 1990;265:7859–7863.

10. Duverger N, Tremp G, Caillaud JM, Emmanuel F, Castro G, Fruchart JC, Steinmetz A, Denefle P. Protection against atherogenesis in mice mediated by human apolipoprotein A-IV. Science 1996;273:966–968.

11. Cohen RD, Castellani LW, Qiao JH, Van Lenten BJ, Lusis AJ, Reue K. Reduced aortic lesions and elevated high density lipoprotein levels in transgenic mice overexpressing mouse apolipoprotein A-IV. J Clin Invest 1997;99:1906–1916.

12. Ostos MA, Conconi M, Vergnes L, Baroukh N, Ribalta J, Girona J, Caillaud JM, Ochoa A, Zakin MM. Antioxidative and antiatherosclerotic effects of human apolipoprotein A-IV in apolipoprotein E-deficient mice. Arterioscler Thromb Vasc Biol 2001;21:1023–1028.

13. Kim H, Mendez R, Zheng Z, Chang L, Cai J, Zhang R, Zhang K. Liver-enriched transcription factor CREBH interacts with peroxisome proliferator-activated receptor alpha to regulate metabolic hormone FGF21. Endocrinology 2014;155:769–782.

14. Nakagawa Y, Satoh A, Yabe S, Furusawa M, Tokushige N, Tezuka H, Mikami M, Iwata W, Shingyouchi A, Matsuzaka T, Kiwata S, Fujimoto Y, Shimizu H, Danno H, Yamamoto T, Ishii K, Karasawa T, Takeuchi Y, Iwasaki H, Shimada M, Kawakami Y, Urayama O, Sone H, Takekoshi K, Kobayashi K, Yatoh S, Takahashi A, Yahagi N, Suzuki H, Yamada N, Shimano H. Hepatic CREB3L3 controls whole-body energy homeostasis and improves obesity and diabetes. Endocrinology 2014;155:4706–4719.

15. Fisher FM, Kleiner S, Douris N, Fox EC, Mepani RJ, Verdeguer F, Wu J, Kharitonenkov A, Flier JS, Maratos-Flier E, Spiegelman BM. FGF21 regulates PGC-1alpha

and browning of white adipose tissues in adaptive ther-mogenesis. Genes & Development 2012;26:271–281.

16. Lin Z, Pan X, Wu F, Ye D, Zhang Y, Wang Y, Jin L, Lian Q, Huang Y, Ding H, Triggle C, Wang K, Li X, Xu A. Fibro-blast growth factor 21 prevents atherosclerosis by sup-pression of hepatic sterol regulatory element-binding protein-2 and induction of adiponectin in mice. Circula-tion 2015;131:1861–1871.

17. Kokkinos J, Tang S, Rye KA, Ong KL. The role of fibro-blast growth factor 21 in atherosclerosis. Atherosclerosis 2017;257:259–265.

18. Liu SQ, Roberts D, Kharitonenkov A, Zhang B, Hanson SM, Li YC, Zhang LQ, Wu YH. Endocrine pro-tection of ischemic myocardium by FGF21 from the liver and adipose tissue. Sci Rep 2013;3:2767.

19. Pan X, Shao Y, Wu F, Wang Y, Xiong R, Zheng J, Tian H, Wang B, Wang Y, Zhang Y, Han Z, Qu A, Xu H, Lu A, Yang T, Li X, Xu A, Du J, Lin Z. FGF21 prevents angio-tensin ii-induced hypertension and vascular dysfunction by activation of ACE2/angiotensin-(1-7) axis in mice. Cell Metab 2018;27:1323–1337 e5.

20. Park JG, Xu X, Cho S, Lee AH. Loss of transcription factor CREBH accelerates diet-induced atherosclerosis in Ldlr-/- mice. Arterioscler Thromb Vasc Biol 2016; 36:1772–1781.

21. Xu X, Park JG, So JS, Hur KY, Lee AH. Transcriptional regulation of apolipoprotein A-IV by the transcription factor CREBH. J Lipid Res 2014;55:850–859.

22. Matthan NR, Giovanni A, Schaefer EJ, Brown BG, Lichtenstein AH. Impact of simvastatin, niacin, and/or antioxidants on cholesterol metabolism in CAD patients with low HDL. J Lipid Res 2003;44:800–806.

23. Kikuchi T, Orihara K, Oikawa F, Han SI, Kuba M, Okuda K, Satoh A, Osaki Y, Takeuchi Y, Aita Y, Matsuzaka T, Iwasaki H, Yatoh S, Sekiya M, Yahagi N, Suzuki H, Sone H, Nakagawa Y, Yamada N, Shimano H. Intestinal CREBH overexpression prevents high-cholesterol diet-induced hypercholesterolemia by reducing Npc1l1 expression. Mol Metab 2016; 5:1092–1102.

24. Nakagawa Y, Oikawa F, Mizuno S, Ohno H, Yagishita Y, Satoh A, Osaki Y, Takei K, Kikuchi T, Han SI, Matsuzaka T, Iwasaki H, Kobayashi K, Yatoh S, Yahagi N, Isaka M, Suzuki H, Sone H, Takahashi S, Yamada N, Shimano H. Hyperlipidemia and hepatitis in liver-specific CREB3L3 knockout mice generated using a one-step CRISPR/Cas9 system. Sci Rep 2016; 6:27857.

25. Chanda D, Kim YH, Li T, Misra J, Kim DK, Kim JR, Kwon J, Jeong WI, Ahn SH, Park TS, Koo SH, Chiang JY, Lee CH, Choi HS. Hepatic cannabinoid receptor type 1 mediates alcohol-induced regulation of bile acid enzyme genes expression via CREBH. PLoS One 2013;8:e68845.

26. Chiang JY. Bile acids: regulation of synthesis. J Lipid Res 2009;50:1955–1966.

27. Schlein C, Talukdar S, Heine M, Fischer AW, Krott LM, Nilsson SK, Brenner MB, Heeren J, Scheja L. FGF21 lowers plasma triglycerides by accelerating lipoprotein catabolism in white and brown adipose tissues. Cell Metab 2016;23:441–453.

28. Lo Sasso G, Murzilli S, Salvatore L, D'Errico I, Petruzzelli M, Conca P, Jiang ZY, Calabresi L, Parini P, Moschetta A. Intestinal specific LXR activation stimu-lates reverse cholesterol transport and protects from atherosclerosis. Cell Metab 2010;12:187–193.

29. Huang Y, He S, Li JZ, Seo YK, Osborne TF, Cohen JC, Hobbs HH. A feed-forward loop amplifies nutritional regulation of PNPLA3. Proc Natl Acad Sci U S A 2010; 107:7892–7897.

30. Wang H, Zhao M, Sud N, Christian P, Shen J, Song Y, Pashaj A, Zhang K, Carr T, Su Q. Glucagon regulates hepatic lipid metabolism via cAMP and Insig-2 signaling: implication for the pathogenesis of hypertriglyceridemia and hepatic steatosis. Sci Rep 2016;6:32246.

31. Yang T, Espenshade PJ, Wright ME, Yabe D, Gong Y, Aebersold R, Goldstein JL, Brown MS. Crucial step in cholesterol homeostasis: sterols promote binding of SCAP to INSIG-1, a membrane protein that facilitates retention of SREBPs in ER. Cell 2002;110:489–500.

32. Satoh A, Han SI, Araki M, Nakagawa Y, Ohno H, Mizunoe Y, Kumagai K, Murayama Y, Osaki Y, Iwasaki H, Sekiya M, Konishi M, Itoh N, Matsuzaka T, Sone H, Shimano H. CREBH improves diet-induced obesity, in-sulin resistance, and metabolic disturbances by FGF21-dependent and FGF21-independent mechanisms. iScience 2020;23:100930.

33. Nakagawa Y, Satoh A, Tezuka H, Han SI, Takei K, Iwasaki H, Yatoh S, Yahagi N, Suzuki H, Iwasaki Y, Sone H, Matsuzaka T, Yamada N, Shimano H. CREB3L3 controls fatty acid oxidation and ketogenesis in synergy with PPARalpha. Sci Rep 2016;6:39182.

34. Wu X, Qi YF, Chang JR, Lu WW, Zhang JS, Wang SP, Cheng SJ, Zhang M, Fan Q, Lv Y, Zhu H, Xin MK, Lv Y, Liu JH. Possible role of fibroblast growth factor 21 on atherosclerosis via amelioration of endoplasmic reticu-lum stress-mediated apoptosis in apoE mice. Heart and Vessels 2014.

35. Zheng Z, Kim H, Qiu Y, Chen X, Mendez R, Dandekar A, Zhang X, Zhang C, Liu AC, Yin L, Lin JD, Walker PD, Kapatos G, Zhang K. CREBH couples circadian clock with hepatic lipid metabolism. Diabetes 2016; 65:3369–3383.

36. Min AK, Jeong JY, Go Y, Choi YK, Kim YD, Lee IK, Park KG. cAMP response element binding protein H mediates fenofibrate-induced suppression of hepatic lipogenesis. Diabetologia 2013;56:412–422.

37. Karasawa T, Takahashi A, Saito R, Sekiya M, Igarashi M, Iwasaki H, Miyahara S, Koyasu S, Nakagawa Y, Ishii K, Matsuzaka T, Kobayashi K, Yahagi N, Takekoshi K, Sone H, Yatoh S, Suzuki H, Yamada N, Shimano H. Sterol regulatory element-binding protein-1 determines plasma remnant lipopro-teins and accelerates atherosclerosis in low-density li-poprotein receptor-deficient mice. Arterioscler Thromb Vasc Biol 2011;31:1788–1795.

38. Ishibashi S, Brown MS, Goldstein JL, Gerard RD, Hammer RE, Herz J. Hypercholesterolemia in low density lipoprotein receptor knockout mice and its reversal by adenovirus-mediated gene delivery. J Clin Invest 1993; 92:883–893.

39. Hotta Y, Nakamura H, Konishi M, Murata Y, Takagi H, Matsumura S, Inoue K, Fushiki T, Itoh N. Fibroblast growth factor 21 regulates lipolysis in white adipose tissue but is not required for ketogenesis and triglyceride clearance in liver. Endocrinology 2009;150:4625–4633.

40. Yakar S, Liu JL, Stannard B, Butler A, Accili D, Sauer B, LeRoith D. Normal growth and development in the absence of hepatic insulin-like growth factor I. Proc Natl Acad Sci U S A 1999;96:7324–7329.

41. Madison BB, Dunbar L, Qiao XT, Braunstein K, Braunstein E, Gumucio DL. Cis elements of the villin gene control expression in restricted domains of the vertical (crypt) and horizontal (duodenum, cecum) axes of the intestine. J Biol Chem 2002;277:33275–33283.

42. Shimano H, Shimomura I, Hammer RE, Herz J, Goldstein JL, Brown MS, Horton JD. Elevated levels of SREBP-2 and cholesterol synthesis in livers of mice homozygous for a targeted disruption of the SREBP-1 gene. J Clin Invest 1997;100:2115–2124.

43. Nakagawa Y, Shimano H, Yoshikawa T, Ide T, Tamura M, Furusawa M, Yamamoto T, Inoue N, Matsuzaka T, Takahashi A, Hasty AH, Suzuki H, Sone H, Toyoshima H, Yahagi N, Yamada N. TFE3 transcriptionally activates hepatic IRS-2, participates in insulin signaling and ameliorates diabetes. Nat Med 2006;12:107–113.

44. Okazaki M, Usui S, Ishigami M, Sakai N, Nakamura T, Matsuzawa Y, Yamashita S. Identification of unique lipoprotein subclasses for visceral obesity by component analysis of cholesterol profile in high-performance liquid chromatography. Arterioscler Thromb Vasc Biol 2005; 25:578–584.

45. Ide T, Shimano H, Yahagi N, Matsuzaka T, Nakakuki M, Yamamoto T, Nakagawa Y, Takahashi A, Suzuki H, Sone H, Toyoshima H, Fukamizu A, Yamada N. SREBPs suppress IRS-2-mediated insulin signalling in the liver. Nat Cell Biol 2004;6:351–357.

46. Yoshikawa T, Ide T, Shimano H, Yahagi N, Amemiya-Kudo M, Matsuzaka T, Yatoh S, Kitamine T, Okazaki H, Tamura Y, Sekiya M, Takahashi A, Hasty AH, Sato R, Sone H, Osuga J, Ishibashi S, Yamada N. Cross-talk between peroxisome proliferator-activated receptor (PPAR) alpha and liver X receptor (LXR) in nutritional regulation of fatty acid metabolism: I—PPARs suppress sterol regulatory element binding protein-1c promoter through inhibition of LXR signaling. Mol Endocrinol 2003; 17:1240–1254.

47. Ide T, Shimano H, Yoshikawa T, Yahagi N, Amemiya-Kudo M, Matsuzaka T, Nakakuki M, Yatoh S, Iizuka Y, Tomita S, Ohashi K, Takahashi A, Sone H, Gotoda T, Osuga J, Ishibashi S, Yamada N. Cross-talk between peroxisome proliferator-activated receptor (PPAR) alpha and liver X receptor (LXR) in nutritional regulation of fatty acid metabolism: II—LXRs suppress lipid degradation

48. Uchida A, Whitsitt MC, Eustaquio T, Slipchenko MN, Leary JF, Cheng JX, Buhman KK. Reduced triglyceride secretion in response to an acute dietary fat challenge in obese compared to lean mice. Frontiers in Physiology 2012;3:26.

49. Fujimoto Y, Nakagawa Y, Satoh A, Okuda K, Shingyouchi A, Naka A, Matsuzaka T, Iwasaki H, Kobayashi K, Yahagi N, Shimada M, Yatoh S, Suzuki H, Yogosawa S, Izumi T, Sone H, Urayama O, Yamada N, Shimano H. TFE3 controls lipid metabolism in adipose tissue of male mice by suppressing lipolysis and thermogenesis. Endocrinology 2013; 154:3577–3588.

gene promoters through inhibition of PPAR signaling. Mol Endocrinol 2003;17:1255–1267.

CRediT Authorship Contributions
Hitoshi Shimano (Conceptualization: Lead; Funding acquisition: Equal; Writing – original draft: Equal; Writing – review & editing: Equal)
   Yoshimi Nakagawa (Conceptualization: Equal; Data curation: Equal; Funding acquisition: Equal; Investigation: Equal; Writing – original draft: Equal; Writing – review & editing: Equal),
   Yunong Wang (Investigation: Equal)
   Song-iee Han (Investigation: Equal)
   Kanako Okuda (Investigation: Equal)
   Asayo Oishi (Investigation: Equal)
   Yuka Yagishita (Investigation: Equal)
   Kae Kumagai (Investigation: Equal)
   Hiroshi Ohno (Investigation: Equal)
   Yoshinori Osaki (Investigation: Equal)
   Yuhei Mizunoe (Investigation: Equal)
   Masaya Araki (Investigation: Equal)
   Yuki Murayama (Supervision: Equal)
   Hitoshi Iwasaki (Supervision: Equal)
   Morichika Konishi (Resources: Equal)
   Nobuyuki Itoh (Resources: Equal)
   Takashi Matsuzaka (Supervision: Equal)
   Hirohito Sone (Investigation: Equal)
   Nobuhiro Yamada (Investigation: Equal)